NASA CR 134694
MDC J6627-01

IMPROVED SOLUTION FOR POTENTIAL FLOW ABOUT ARBITRARY AXISYMMETRIC BODIES BY THE USE OF A HIGHER-ORDER SURFACE SOURCE METHOD

PART I. THEORY AND RESULTS

John L. Hess and Robert P. Martin, Jr.

DOUGLAS AIRCRAFT COMPANY

prepared for

NATIONAL AERONAUTICS AND SPACE ADMINISTRATION

NASA Lewis Research Center
Contract NAS3-18018

1. Report No.	2. Government Accession No.	3. Recipient's Catalog No.
NASA CR 134694		

4. Title and Subtitle	5. Report Date
Improved Solution for Potential Flow about Arbitrary Axisymmetric Bodies by the Use of a Higher-Order Surface Source Method. Part I. Theory and Results	July 1974
	6. Performing Organization Code

7. Author(s)	8. Performing Organization Report No.
John L. Hess and Robert P. Martin, Jr.	MDC J6627-01
	10. Work Unit No.

9. Performing Organization Name and Address	11. Contract or Grant No.
Douglas Aircraft Company McDonnell Douglas Corporation Long Beach, California 90846	NAS3-18018
	13. Type of Report and Period Covered

12. Sponsoring Agency Name and Address	13. Type of Report and Period Covered
National Aeronautics and Space Administration Lewis Research Center Cleveland, Ohio 44135	Contractor Report
	14. Sponsoring Agency Code

15. Supplementary Notes

Project Manager, James A. Albers
NASA Lewis Research Center, Cleveland, Ohio

16. Abstract

The well-known surface-source method of calculating potential flow can be improved by refining the underlying numerical analysis. Instead of approximating a body contour by straight-line elements on each of which the source density is constant, the present analysis uses parabolic elements and linearly-varying source density. The result is a large increase in computing speed and accuracy.

This report describes the theory and presents a number of calculated results to illustrate the effectiveness of the modification.

17. Key Words (Suggested by Author(s))		18. Distribution Statement
Aerodynamics	Higher-order method	Unclassified - unlimited
Axisymmetric bodies	Numerical analysis	
Computer program	Pressure distribution	
Flow field	Surface singularity	
Fluid dynamics		

19. Security Classif. (of this report)	20. Security Classif. (of this page)	21. No. of Pages	22. Price*
Unclassified	Unclassified		

*For sale by the National Technical Information Service, Springfield, Virginia 22151

FOREWORD

The enthusiastic assistance of Mrs. Sue Schimke was a highly significant factor in the successful completion of this work. While her contributions were appreciated at all stages of the development, her running and analyzing of the various test cases was especially important.

TABLE OF CONTENTS

SUMMARY

In recent years the surface-source method of calculating potential flow about arbitrary bodies has been developed extensively and has proved to be a useful tool in a wide variety of low-speed design applications ranging from simple shapes to complicated inlets with centerbodies, multielement airfoils, and wing-fuselage-pylon-nacelle combinations. Two-dimensional, axisymmetric, and three-dimensional methods have been developed. While the method is generally quite satisfactory, increases in computational speed and accuracy are desirable for certain applications, particularly interior flows and exterior flows about complicated multiple-body combinations. Such improvements can be realized by refining the formulation. In the basic method the profile curve of a two-dimensional or axisymmetric body is approximated by a large number of straight-line elements over each of which the source density is constant. The so-called higher-order refinement consists of using curved surface elements and a source density that varies over an element. This report describes the analysis for the axisymmetric case where the next-simplest approximation is used. Specifically, the surface elements are parabolas, and the source density varies linearly in arc length over each element. Calculated results for a series of test cases are presented and compared. For both exterior and interior flows the higher-order formulation yields very significant decreases in computing time and increased computational accuracy.

LIST OF SYMBOLS

a	radius of a ring source or vortex
b	axial location of a ring source or vortex
c	half the curvature of an element
C	cy
i,j	integer subscripts denoting particular elements
N	total number of elements on a body
s	arc length along an element
s'	half the total arc length of an element
S'	s'y
V	surface velocity
V_∞	free-stream velocity
V_x, V_y	velocity components
$\bar{V}$	velocity due to a ring source or vortex
$\bar{V}_i$	perturbation velocity at i-th control point
$\bar{V}_{ij}$	velocity at i-th control point due to a unit value of j-th source density with all other values zero
$\bar{V}^*_{ij}$	velocity at i-th control point due to a parabolic source density distribution on the j-th element
x	axial coordinate
$\bar{x}$, $\bar{y}$	coordinates of a control point
y	radial coordinate
α	slope angle of the tangent to an element at the control point with respect to the x-axis
Δ	length of the chord of an element
n_o	perpendicular distance from control point to chord of an element

θ	circumferential angle about the x-axis
μ	vorticity strength
ξ, η	Cartesian coordinates with origin at the control point of an element and directions, respectively, parallel and perpendicular to the tangent line
σ	source density
$\sigma^{(1)}$	derivative of source density with respect to arc length
$\sigma^{(2)}$	half the second derivative of source density with respect to arc length
ϕ	velocity potential

INTRODUCTION

Recent years have seen the development of very general surface singularity methods for the calculation of potential flow about arbitrary configurations [1]. Moreover, these methods have been applied successfully to a large number of practical design problems of low-speed flow [1], [2]. The most common such method is the so-called surface-source method [2], which utilizes a source density distribution over the surface of the body about which flow is to be computed. Application of the boundary condition of zero (or prescribed) normal velocity on the body surface theoretically yields a Fredholm integral equation of the second kind for the source density. Once the source density is known, all other quantities, such as flow velocities and pressures, may be obtained by integration. Separate procedures have been developed for calculating flow about two-dimensional bodies, axisymmetric bodies, and three-dimensional bodies, respectively. For the case of axisymmetric bodies the flow itself does not necessarily have axisymmetric, but it may be a case of cross flow for which the free-stream direction is perpendicular to the body's symmetry axis or a case of rotation of the body about an axis perpendicular to its symmetry axis [2].

To implement this method for the computer, various approximations must be made. In particular, both the body shape and the source density distribution must be approximated in a form suitable for machine computation. During most of the development of the surface-source method the profile curve defining an axisymmetric (or two-dimensional) body has been approximated by a large number N of small straight-line elements, which form an inscribed polygon. Moreover, the source density has been assumed to be constant over each straight-line element, although it varies from one element to another. This reduces the problem of determining the source density distribution to that of determining a finite number of values of the source density — one for each element. One point of each element, the midpoint for a straight-line element, is selected as the control point where the normal-velocity boundary condition is to be applied. Formulas have been derived that give the velocity at any point due to a unit value of source density on a straight-line element. From these formulas a matrix of vector velocities induced by the elements at the control points can be obtained. Then the integral equation is replaced by a set of linear algebraic equations for the values of source density on the elements. The coefficient matrix of this set of equations consists of the set of normal velocities induced by the elements at each others' control points, which is obtained by taking normal components of the basic induced velocity matrix. Finally, surface velocities at the control points are obtained by a matrix multiplication of the tangential components of the induced velocity matrix with the column of values of source density. The two main parts of the computation are the calculation of the N^2 velocities that comprise the induced velocity matrix and the solution of the linear equations for the values of source density. If a direct elimination solution is used, the computational magnitude of solving the linear equations is proportional to N^3.

The above described procedure, which uses flat surface elements and a piecewise-constant source density distribution, is designated the base method. It has proved satisfactory in a wide variety of design applications [1],[2]. However, it is evident that more elaborate procedures can be formulated and

that these should give a higher accuracy for a given element number N and thus an equal accuracy with a smaller element number. Moreover, if it is properly implemented, a more elaborate procedure would require only a slightly greater computing time than the base method for a given N. Because of the rapid variation of computing time with N, a reduction of computing time for a given accuracy should be possible. This has been successfully accomplished for the case of two-dimensional bodies [1], [3], [4], [5], in which case the application of main interest is a multielement airfoil. Here the case of axisymmetric bodies is considered, where the application of main interest is an inlet, possibly with centerbody and ring vanes. The technique employed is basically the one used in two dimensions [3], which employs curved surface elements and a source density that varies over the element. Such an approach is designated a higher-order implementation. For axisymmetric bodies these variations refer to the profile curve defining the body. The circumferential variations around the symmetry axis of element geometry and source density are similar to those of the base method [2]. Namely, a complete surface element is a portion of a conoid (a cone frustum in the flat-element case), and the source density is independent of circumferential angle for axisymmetric flow and is proportional to the cosine of the circumferential angle for cross flow and for rotation.

Use of higher-order implementations brings up the question of the consistency of the orders of the approximation used for the element geometry and the approximation used for the source density. It is known [1], [3], that consistency is obtained when the polynomial expressing the element shape has a degree one higher than that defining the source density. Thus, consistent formulations include: (1) flat-element constant-source, (2) parabolic-element linear-source, and (3) cubic-element parabolic-source. In this paper parabolic elements are used together with a piecewise-parabolic source density. The extra inconsistent parabolic term in the source density has been included to determine whether or not it gives increased accuracy in low-curvature regions. It turns out that, as the theory predicts, little or no gain in accuracy is obtained by including the parabolic source term.

SURFACE ELEMENT GEOMETRY

The profile curve of the body about which flow is to be computed is specified as a table of coordinates for $N + 1$ points (x_i, y_i), each of which is presumably exactly on the contour. By this means the contour is divided into N elementary arcs as shown in Figure 1. On each arc a control point is selected by the following criterion: the normal projections of the endpoints of the element, (x_i, y_i) and (x_{i+1}, y_{i+1}), on the line tangent to the arc at the control point are equidistant from the control point. The slope of the tangent line at the control point is defined as the slope of the element. If this tangent line is taken as the horizontal axis of a ξ,η-coordinate system with the control point as origin, the elementary arc is as shown in Figure 2. The equation of this arc may be written as a power series

$$\eta = c\xi^2 + \ldots \tag{1}$$

The arc length s along the arc measured from the control point is given by

$$\begin{aligned} ds &= \left[\sqrt{1 + (2c\xi)^2 + \ldots}\right]d\xi \\ &= [1 + 2c^2\xi^2 + \ldots]d\xi \end{aligned} \tag{2}$$

Thus

$$s = \xi + \frac{2}{3}c^2\xi^3 + \ldots \tag{3}$$

The basic reference coordinate system in which the body is defined has its x-axis as the symmetry axis of the body. Let a point of the element have coordinates $x = b$ $y = a$ in this system then

$$\begin{aligned} b &= \bar{x} + (\cos\alpha)\xi - c(\sin\alpha)\xi^2 + \ldots \\ a &= \bar{y} + (\sin\alpha)\xi + c(\cos\alpha)\xi^2 + \ldots \end{aligned} \tag{4}$$

where α is the slope angle of the ξ-axis (tangent line) with respect to the x-axis and $\bar{x}, \bar{y}$ are reference coordinates of the control point.

In principle, approximations of arbitrarily high order could be generated by retaining surfficient terms in the above series. For present purposes the element is assumed to be parabolic, and the above series are terminated with the terms shown. For this approximation the control point lies on the perpendicular bisector of the straight line between (x_i, y_i) and (x_{i+1}, y_{i+1}) and the slope of the element equals the slope of this straight line. Also, by inspection of (3) it can be seen that to this order of approximation s may be substituted for ξ in (4). A circle is passed through the points (x_{i-1}, y_{i-1}), (x_i, y_i), and (x_{i+1}, y_{i+1}), and another circle is passed through the points

(x_j, y_j), (x_{j+1}, y_{j+1}) and (x_{j+2}, y_{j+2}). The half-curvature c of the parabolic element, which enters equations (1) and (4), is set equal to half the geometric mean of the curvatures of these two circles. Requiring the parabola to pass through the endpoints (x_j, y_j) and (x_{j+1}, y_{j+1}) then uniquely defines the parabola and establishes the coordinates $\bar{x}, \bar{y}$ of the control point. For the first and last elements of a body one circle is not defined and c is set equal to half the curvature of the remaining circle.

Explicit formulas for the above procedure are contained in Appendix A.

INDUCED VELOCITY MATRICES

The basic calculational task of the flow-calculation method is to compute the flow velocities induced by the elements at each others' control points. There are three types of induced velocities corresponding to three types of surface singularity: (1) a constant-strength ring source, which is appropriate for axisymmetric flow; (2) a ring source whose strength is proportional to the cosine of the circumferential angle, which is appropriate for cross flow and for body rotation; and (3) a constant-strength ring vortex, which is used to produce certain auxiliary solutions appropriate to axisymmetric flow about ring-airfoils and inlets. The velocities in the induced velocity matrices are obtained by integrating the ring source or vortex formulas over an element. Specifically, let a ring singularity (source or vortex) have a radius a and lie in the plane $x = b$ with its center on the x-axis. Then the velocity at the point (x,y) due to this singularity is

$$\vec{V} = \vec{V}[x, y, b, a] \tag{5}$$

Specific formulas for the two types of ring source are contained in [2] and derived in [6], [7]. Many of the functions appearing in the expressions are repeated, particularly the specific complete elliptic integrals. The velocity components of a constant-strength ring vortex are related to those of a constant-strength ring source by [8]

$$\begin{aligned} V_x(\text{vortex}) &= \frac{a^2 - y^2}{a(x-b)} V_x(\text{source}) + \frac{y}{a} V_y(\text{source}) \\ V_y(\text{vortex}) &= \frac{y}{a} V_x(\text{source}) - \frac{x-b}{a} V_y(\text{source}) \end{aligned} \tag{6}$$

Let the source density on the j-th element be denoted $\sigma_j(s)$. The velocity induced by this source density at control point of the i-th element $(\bar{x}_i, \bar{y}_i)$ is obtained by integrating over the element, that is

$$\vec{V}^*_{ij} = \int_{\Delta s_j} \vec{V}[\bar{x}_i, \bar{y}_i, b_j(s), a_j(s)]\sigma_j(s)ds \tag{7}$$

where Δs_j is the total arc length of the j-th element. Equation (7) applies to both types of source singularity. This equation also applies to the vorticity singularity if $\sigma_j(s)$ is replaced by the vorticity strength $\mu_j(s)$. In evaluating the integral of (7), b and a are given by (4) with s replacing ξ.

The source density may be written as a power series

$$\sigma_j(s) = \sigma_j + \sigma_j^{(1)}s + \sigma_j^{(2)}s^2 + \ldots \tag{8}$$

where σ_j, $\sigma_j^{(1)}$ and $\sigma_j^{(2)}$ are independent of s and represent, respectively, the value, first derivative, and half the second derivative of the source density at the control point of the j-th element. In the present analysis the source density is assumed to be at most parabolic, and (8) is terminated with the terms shown. Thus (7) becomes

$$\vec{V}^*_{ij} = \sigma_j \int_{\Delta s_j} \vec{V}[\bar{x}_i, \bar{y}_i, b_j(s), a_j(s)]ds$$

$$+ \sigma_j^{(1)} \int_{\Delta s_j} \vec{V}[\bar{x}_i, \bar{y}_i, b_j(s), a_j(s)]sds \qquad (9)$$

$$+ \sigma_j^{(2)} \int_{\Delta s_j} \vec{V}[\bar{x}_i, \bar{y}_i, b_j(s), a_j(s)]s^2ds$$

or

$$\vec{V}^*_{ij} = \vec{V}^{(0)}_{ij}\sigma_j + \vec{V}^{(1)}_{ij}\sigma_j^{(1)} + \vec{V}^{(2)}_{ij}\sigma_j^{(2)} \qquad (10)$$

The vorticity distribution $\mu_j(s)$ is taken as constant so that only the first terms of (9) and (10) are present. In fact, the vorticity is handled exactly as in the base method [1], except that the integral is over a curved element rather than a flat one. The form of equation (10) makes it easy to investigate the effectiveness of retaining various terms in the source density expansion. The relative effectiveness of flat and curved elements can be investigated by setting c either zero or nonzero in equation (4).

For $j \neq i$ the integrals in (9) are evaluated by numerical integration using Simpson's rule with a variable number of ordinates [2]. It is evident from (9) that the three integrands are very similar and can be conveniently calculated together. For $j = i$ the basic ring-source (or vortex) velocity $\vec{V}[x,y,b,a]$ has a singularity of order $1/s$ at $s = 0$. Accordingly, resort must be made to a series expansion in powers of s so that the singularity may be cancelled analytically. These expansions are similar to those used in the base method [2]. The quantities $\vec{V}[x,y,b,a]s$ and $\vec{V}[x,y,b,a]s^2$ are not singular but for consistency they are evaluated by series expansions for $j = i$. Derivation of these expressions is straightforward but tedious and is not pursued here. Formulas for these expansions are contained in Appendix B.

ORGANIZATION OF THE CALCULATION

In the most general case all three integrals of equation (9) must be evaluated for both the axisymmetric and the cross-flow type of source density. Thus including the vorticity, which requires only the first integral of (9), there are seven vector integrals in the higher-order analysis as opposed to three in the base method. In axisymmetric flow there are two velocity components, axial and radial, while cross flow has an additional circumferential component. Thus the total number of scalar integrals can be seventeen rather than the seven of the base method. However, the final number of scalar N x N induced velocity component matrices that must be stored and used is the same in the higher order and base methods, namely five.

As described above, the normal velocity boundary condition is applied at the control point of each element to produce a number of linear equations equal to the number of elements. However, the variation of source density over an element is described by three parameters, σ_j, $\sigma_j^{(1)}$, and $\sigma_j^{(2)}$. The derivatives $\sigma_j^{(1)}$ and $\sigma_j^{(2)}$ are expressed in terms of values of σ by differentiating the parabola through the three values σ_{j-1}, σ_j, and σ_{j+1}. That is

$$\sigma_j^{(1)} = D_j\sigma_{j-1} + E_j\sigma_j + F_j\sigma_{j+1}$$
$$\sigma_j^{(2)} = G_j\sigma_{j-1} + H_j\sigma_j + I_j\sigma_{j+1} \qquad (11)$$

where the coefficients in (11) are standard numerical differentiation formulas and depend only on the lengths of the three elements [3]. For the first (or last) element of a body the parabola that is differentiated passes through the first (or last) three values of σ, and the formulas of (11) are modified accordingly. This last feature could introduce error if a smooth contour is defined with the first and last points coincident, as for example, a torous. However, this case is too rare to be of great significance. The above procedure is appropriate for all inlets and ducts and also for simply-connected bodies, which are input from the upstream stagnation point to the downstream stagnation point.

From (10) and (11) it is evident that the velocity induced at a point by an element is a linear combination of three neighboring values of σ. The matrix that is needed for subsequent calculations is the one giving the velocity at each control point due to each value of source density. As the calculation proceeds to calculate the velocity at a control point due to successive elements, the velocity induced by the j-th element is not associated entirely with σ_j as in the base method, but certain portions are associated with σ_{j-1}, σ_j, and σ_{j+1} in the obvious way. When all elements have been accounted for, the velocity at a control point due to each value of source density has been formed as the sum of contributions from three elements except for those due to the first and last values, to which two elements contribute and then those due to the third and third-to-last values, to which four elements contribute. The result of this phase of the computation is a matrix $\bar{V}_{ij}$, such that the velocities at the control points due to the body are

$$\vec{V}_i = \sum_{j=1}^{N} \vec{V}_{ij}\sigma_j, \qquad i = 1, 2, \ldots, N \qquad (12)$$

There is a single vector matrix $\vec{V}_{ij}$ for the axisymmetric source densities, one for the cross-flow source densities, and one for the axisymmetric vorticities, just as in the base method. Moreover, as in the base method, the vortex velocities are not saved individually. Instead the velocities produced by all elements at a control point are added together to give the velocity at that control point due to a vortex sheet of constant unit strength. This auxiliary onset flow is used in certain inlet and ring-wing applications.

Thus the result of this phase of the calculation is a set of matrices $\vec{V}_{ij}$ and vorticity onset-flows equivalent to those of the base method. In fact, all subsequent calculations [2] are identical for both base and higher-order methods and do not depend on how the $\vec{V}_{ij}$ matrix was produced. In particular, the normal component of $\vec{V}_{ij}$ is the coefficient matrix of the linear equations for the values of source density. The right sides of these equations are the negatives of the normal components of the onset flows, either uniform or otherwise. Once solutions have been obtained, the flow velocity at each control point (or any other point) is calculated for each onset flow by adding a sum of the form (12) to the onset-flow velocity at that point.

Explicit coefficients for the numerical differentiation formula (11) are presented in Appendix C.

DISCUSSION OF RESULTS

Comparison of Calculated Results with Analytic Solutions

To determine the effectiveness of the higher-order technique and to evaluate the importance of the various terms in the expansion, a considerable number of calculations have been performed for a sphere and for a 8-to-1 prolate spheroid, for which analytic solutions are available. The first conclusion that can be drawn from these calculations is that the addition of the quadratic source density term $\sigma_j^{(2)}$ never yields an appreciable increase in accuracy regardless of whether flat or curved surface elements are used. In every case the solution that utilizes only σ_j and $\sigma_j^{(1)}$ is virtually indistinguishable from the one that also includes $\sigma_j^{(2)}$. In what follows, the solution that utilizes curved surface elements and a linearly varying source density is denoted "higher order" while the flat-element constant-source solution is denoted the base method. Solutions obtained with other combinations of terms are labeled explicitly.

Calculations were performed for a sphere represented by 60 equal-length elements of 3° subtended angle. Four solutions were obtained. In addition to the higher order and the base method, two inconsistent solutions were obtained: that using the curved-elements constant-sources and that using flat-elements linear-sources. The higher-order solution was also calculated for a 12-element sphere whose elements each subtend a 15° angle. Results for a uniform onset flow parallel to the x-axis are presented in Figure 3, which shows differences between calculated and analytic surface velocities. The importance of mathematical consistency is evident. Accounting for either source variation or element curvature separately produces no improvement on the base method. However, when both are accounted for, as in the higher-order solution, the result is a large gain in accuracy — about two orders of magnitude. Even the 12-element higher-order solution is an order of magnitude more accurate than the 60-element base method and also requires an order of magnitude less computing time.

If the uniform onset flow is parallel to the y-axis, i.e., a "cross flow," the calculated results are slightly different from those for the case of onset flow parallel to the x-axis, because in the former case the conoidal surface elements do not have the same axis of symmetry as the flow field. Errors in calculated surface velocities are shown in Figure 4. Figure 4a shows velocities along the profile curve in the plane containing the onset flow vector and the body's symmetry axis (xy-plane). Figure 4b shows velocities along the curve in the plane perpendicular to the onset flow and containing the body's symmetry axis (xz-plane). In this last plane the analytic velocity has a constant value of 1.5 and is parallel to the onset flow vector. The gain in accuracy from use of the higher-order solution is not as impressive in Figure 4a as it is in Figure 3, but it is still present. In particular the 12-element higher-order solution is still at least as accurate as the 60-element base method. The ineffectiveness of the two inconsistent solutions is quite clear. The results of Figure 4b are similar, with one exception, to those of Figure 3. Both the 60-element and the 12-element higher-order solutions are much more accurate than the 60-element base method. However, unlike the case of Figure 3, the gain in accuracy of Figure 4b is due largely to the use of curved elements

while the use of a variable source density has virtually no effect. However, the fact that this is true for one velocity component out of three does not change the basic conclusion that in general a consistent formulation is required to obtain a significant increase in accuracy.

The relative effectiveness of the two methods of solution for an 8-to-1 prolate spheroid is illustrated in comparing results for the base method using 60 elements with results for the higher-order method using 30 elements. For these element numbers the higher-order method is approximately four times faster than the base method. Somewhat different distributions of elements are used for the two methods. The distribution used for the higher-order method concentrates elements in the high-curvature region to a greater degree than that for the base method. Correspondingly, the higher-order solution uses very few elements in the low-curvature region, but it is able to maintain accuracy in this region because of the use of variable source density. Generally, each method is used with the element distribution for which the best solution is obtained. (Similar experience is reported in [3].) Differences between calculated and analytic surface velocities are shown in Figure 5 for the axisymmetric case where the onset flow is parallel to the body's symmetry axis (x-axis) and in Figure 6 for the cross-flow case where the onset flow is perpendicular to the body's symmetry axis (parallel to the y-axis). To put these results in perspective, the maximum value of surface velocity is about 1.0293 times free-stream velocity for the axisymmetric case of Figure 5 and about 1.9447 times free-stream velocity for the cross-flow case of Figure 6. In the xz-plane, Figure 6b, the velocity is parallel to free-stream and has a constant magnitude of 1.9447. The curves of Figures 5 and 6 emphatically show that in addition to being much faster the higher-order technique is also much more accurate than the base method. The substantial gain in accuracy that can be achieved by use of the higher-order method for cases of smooth convex bodies is in marked contrast to the two-dimensional case [3].

Interior Flow in Ducts

In two dimensions [4] the greatest gains in accuracy from use of the higher-order method occur for interior flow in ducts. To investigate the behavior of the present axisymmetric case, the first geometry selected is the analog of one previously considered in [3], namely the case of a uniform onset flow into the closed duct shown in Figure 7 (an interior hemisphere cylinder). The flow inside the duct should be virtually stagnant, and the average axial velocity component at any axial location should be exactly zero. Thus, the average axial velocity is a measure of the calculational error. The base method with 55 elements gives a typical error of 15 percent of free-stream velocity. Use of the higher-order technique reduces this error by a full two orders of magnitude.

A more practical case is that of a contracting duct of area ratio 16 as shown in Figure 8. The contracting section is a portion of a sine wave. By continuity the net flux of fluid at every axial station should be identical, so changes in this flux represent calculational error. Net fluxes have been calculated at five stations as shown in Figure 8 and normalized with respect to the flux in the large constant-diameter section. It is evident that the

use of the higher-order solution reduces the maximum error in flux by a factor of about 25.

Inlets

The most frequently-occurring type of axisymmetric body is an inlet. Simulating an arbitrarily prescribed mass flow ratio through the inlet requires use of an artifice that is described in detail in Appendix D. Basically, three flow solutions are required: that about the empty inlet in a uniform onset flow at zero angle of attack (Figure 9a), the pure cross-flow due to a uniform stream at 90° angle of attack (Figure 9b), and a static solution, where there is flow through the inlet but no onset flow. This last solution can be obtained either by the use of an interior suction surface (Figure 10a) or by use of surface vorticity (Figure 10b). The first two solutions are no more difficult than those for flow about simple closed bodies. It is the static solution that can lead to numerical difficulty and may require large element numbers.

Several inlet goemetries were studied with both the higher-order solution and the base method for two or three different element numbers. Since results for all inlets are similar, discussion here is concentrated on the results for the inlet-centerbody combination shown in Figure 11. The control station where mass flow ratios are evaluated is at $x = 13.4$ and the inlet is terminated at $x = 44$, about two diameters. Figure 12a shows an input point distribution typical of those customarily used to define such an inlet — a total of 244 elements. The element number has been reduced by deleting every other input point in the forward region, but the same element size is maintained on the afterbody. The resulting input point distribution, which corresponds to 149 elements, is shown in Figure 12b. The same procedure was applied to the distribution of Figure 12b to produce the 103-element distribution of Figure 12c, which has only one-fourth the density in the nose region as that of Figure 12a.

The most surprising result of the calculations for all inlets and for both the higher-order and the base method is that the calculated velocity distributions do not change much with element number. Thus, if a user contemplated a series of cases, it would be profitable for him to do a little initial experimentation with element number and select the lowest possible.

With regard to flow continuity inside the inlet, the higher-order solution is an order of magnitude more accurate than the base method, but the latter is accurate enough for most purposes. The only real advantage in this regard for the higher-order solution is that its control station may be located anywhere, while the base method should have its control station as far forward as possible.

The higher-order solution and the base method give virtually identical results for the two solutions of Figure 9. This was not unexpected. However, for the static solution of Figure 10, the higher-order solution offers an improvement in accuracy over the base method for the same element number. The improvement is modest if the surface-vorticity method of generating a static solution (Figure 10b) is used, but is quite substantial if the interior suction method (Figure 10a) is used.

When the surface vorticity solution for the inlet of figure 11 was calculated, the 244-element and the 149-element higher-order solutions gave graphically identical velocity distributions, which may be regarded as the "correct" answer. This is compared in Figure 13 with: the 103-element higher-order, the 103-element base method, and the 244-element base method. The 103-element higher-order solution is clearly superior to the 103-element base method and is at least comparable to and probably superior to the 244-element base method, which requires at least six times as much computing time.

The suction method of simulating a static case (Figure 10a) was calculated with 149 elements for both the higher-order solution and the base method. For both solutions the suction element was placed at $x = 44$. The resulting velocity distributions are compared with the "correct" (i.e., 244-element higher order) solution of Figure 14. It is evident that the higher-order solution effects a considerable increase in accuracy on the inside of the inlet. In fact, the very close agreement of the two quite different higher-order solutions of Figure 14 is further evidence that the 244-element (or 149-element) higher-order solution with surface vorticity is indeed the "correct" static solution. However, on the outside of the inlet the difficulties associated with suction solutions (Appendix D) are evident. Rather than a montonically decreasing velocity of constant direction (towards the inlet lip) the suction solutions have stagnation points aft of which the flow is in the wrong direction. Moreover, the higher-order solution is not much better than the base method. Aft of the ficticious stagnation point of the static solution the calculated variation of surface pressure with mass flow ratio has the opposite sign from the true variation. Thus, if the outside of the inlet is of interest, the surface vorticity method of simulating a static solution should be used in preference to the suction method. The previous statement is true for all inlets where the outside surface is essentially parallel to the inside surface at aft locations (Figure 11). It does not hold for "bellmouth" or "flush" inlets, which are characterized by the fact that the outside surface does not bend around and eventually assume a constant radius (constant value of y) but instead proceeds radially outward to large distances at a nearly constant value of x. For these inlets, the suction method and the surface vorticity method of simulating the static solution are essentially equivalent.

CONCLUSIONS

The higher-order method (parabolic-element linear-source) is both faster and more accurate than the base method (straight-line-element constant-source) for exterior flow about simple bodies and for interior flow in ducts. The precise amount of improvement depends on the body shape and on the velocity component considered, but an order of magnitude improvement in both speed and accuracy has been obtained in apparently typical cases.

For inlet flows the effectiveness of the higher-order method is less dramatic, but it still appears to offer some improvement over the base method.

Use of a surface vorticity distribution to generate a static solution for inlets is much preferable to use of an interior suction surface.

Satisfactory results can be obtained in inlet cases with fewer elements than is currently customary.

APPENDIX A
ELEMENT GEOMETRY FORMULAS

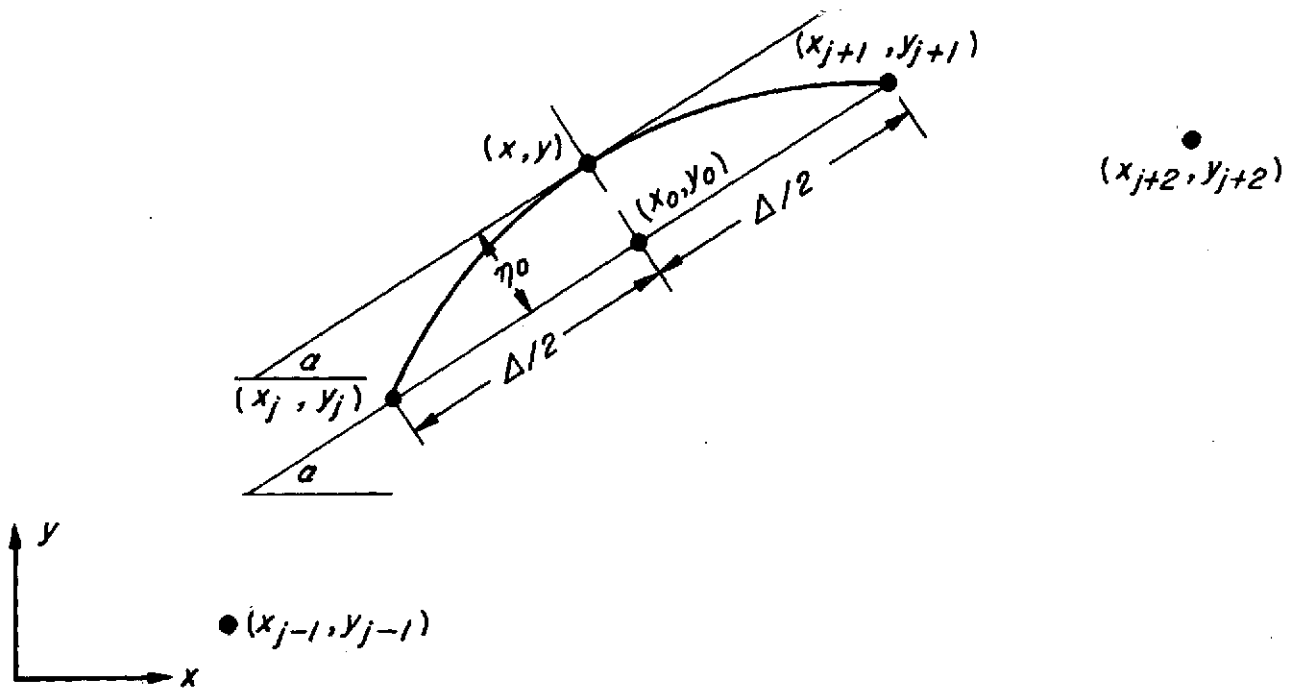

As in the present program the following geometric quantities associated with the j-th element are computed from two adjacent input points (x_j, y_j) and (x_{j+1}, y_{j+1}).

$$x_0 = \frac{1}{2}(x_j + x_{j+1})$$

$$y_0 = \frac{1}{2}(y_j + y_{j+1})$$

$$\Delta = \sqrt{(x_{j+1} - x_j)^2 + (y_{j+1} - y_j)^2} \qquad \text{(A-1)}$$

$$\cos\alpha = \frac{x_{j+1} - x_j}{\Delta}$$

$$\sin\alpha = \frac{y_{j+1} - y_j}{\Delta}$$

Now the element curvature must be computed. Half the value of curvature is stored. The half curvature is denoted c. However, the actual curvature 2c is printed out on the preliminary output. This is the only addition to that output. The curvature of the j-th element is computed as the geometric mean of the curvatures of two circles: the "left" circle through the points (x_{j-1}, y_{j-1}), (x_j, y_j), and (x_{j+1}, y_{j+1}) and the "right" circle through the points (x_j, y_j), (x_{j+1}, y_{j+1}), and (x_{j+2}, y_{j+2}). If the "left" and "right" circles have curvatures of opposite sign, the element curvature is set equal to zero. The above scheme will not work for the first and last elements of a body. For the first element the curvature is set equal to that of the "right" circle and the (nonexistent) "left" circle is ignored. For the last element the curvature is set equal to that of the "left" circle and the (nonexistent) "right" circle is ignored. This scheme is proper for the overwhelming majority of bodies: (1) finite body on axis, e.g., a sphere, (2) semi-infinite body on axis, e.g., a hemisphere cylinder, (3) a semi-infinite body off the axis, e.g., an inlet, (4) a duct, and (5) a ring airfoil with sharp trailing edge. The only exception is the smooth "donut type" body for which it would be preferrable to form a "left" circle for the first element using the second-to-last input point and a "right" circle for the last element using the second input point. However, this case does not seem to be important enough to justify an option.

The basic calculational unit of the above is the computation of the curvature of a circle through three given points. Let the points through which the circle goes be (x_1, y_1), (x_2, y_2), (x_3, y_3). The order of the points is important, because it determines the sign of the curvature. In the present application the curvature is negative on convex portions of the body. The curvature 2c is

$$2c = \frac{D}{R} \tag{A-2}$$

where

$$\begin{aligned} D &= 4[(x_2 - x_1)(y_2 - y_3) - (x_2 - x_3)(y_2 - y_1)] \\ R &= \sqrt{(Dx_2 - D_n)^2 + (Dy_2 - D_k)^2} \\ D_n &= 2[(x_1^2 + y_1^2)(y_3 - y_2) + (x_2^2 + y_2^2)(y_1 - y_3) + (x_3^2 + y_3^2)(y_2 - y_1)] \\ D_k &= 2[(x_1^2 + y_1^2)(x_2 - x_3) + (x_2^2 + y_2^2)(x_3 - x_1) + (x_3^2 + y_3^2)(x_1 - x_2)] \end{aligned} \tag{A-3}$$

Once the curvature is known the offset distance η_0 (see sketch above) is determined by passing a symmetric parabola with that curvature at the vertex through the endpoints. This gives

$$\eta_0 = -c\,\frac{\Delta^2}{4} \tag{A-4}$$

Then the control point coordinates are

$$\bar{x} = x_0 - \eta_0 \sin \alpha$$
$$\bar{y} = y_0 + \eta_0 \cos \alpha \qquad \text{(A-5)}$$

These now replace x_0 and y_0, which are discarded. The control point $(\bar{x}, \bar{y})$ also serves as the origin of element coordinates.

The "half" arc length s' of the curved element is obtained from

$$s' = \frac{\Delta}{2}\left(1 + \frac{1}{6} c^2 \Delta^2\right) \qquad \text{(A-6)}$$

The arc length Δs on the Basic Case output is

$$\Delta s = 2s' \qquad \text{(A-7)}$$

All integrations versus arc length used to construct the induced velocity matrices have integration limits of $-s'$ to $+s'$.

There is also an option to input curvatures for each element. If this option is used, the curvature computation is bypassed, and a table of curvatures for all elements of all bodies is input. These are divided by two to produce the half curvatures c, which are stored with the basic geometric data for each element. Quantities saved for each element are

$$\bar{x},\ \bar{y},\ c,\ \Delta,\ \sin \alpha,\ \cos \alpha,\ s' \qquad \text{(A-8)}$$

APPENDIX B

SINGULAR SUBELEMENT EXPANSIONS

The logical structure of this calculation is described in [2], [6], [7]. First the half arc length s' is tested. If

$$s' \leq 0.08\ \bar{y} \tag{B-1}$$

then the effect of the entire element is given by the singular subelement series (discussed below) and the argument of this series S' is

$$S' = s'/\bar{y} \tag{B-2}$$

If on the other hand,

$$s' > 0.08\ \bar{y} \tag{B-3}$$

then the effect of the "middle" of the element, i.e., the portion

$$-0.08\bar{y} < s < 0.08\ \bar{y} \tag{B-4}$$

is given by the singular subelement series with argument

$$S' = 0.08 \tag{B-5}$$

The "ends" of the element, i.e., the two portions

$$-s' < s < -0.08\ \bar{y} \qquad \text{and} \qquad 0.08\ \bar{y} < s < s' \tag{B-6}$$

are treated as two off-diagonal elements and their effects are computed by the numerical integration scheme of the section Induced Velocity Matrices.

The required singular subelement series are logically similar to those of the base method, which they replace. These series are listed on the following pages, equations (B-9), (B-10), (B-11), (B-12), (B-13), (B-14), and (B-15). The only new parameter in these equations is

$$C = c\bar{y} \tag{B-7}$$

These equations lack the additional $2\pi\sigma_j$ normal velocity term. Thus, these terms must be added to the coefficient of σ_j. (The coefficients of $\sigma_j^{(1)}$ and $\sigma_j^{(2)}$ are not affected.) The terms to be added are:

Axisymmetric	x : $2\pi \sin\alpha$	
	y : $-2\pi \cos\alpha$	
Cross Flow	x : $2\pi \sin\alpha$	
	y : $-2\pi \cos\alpha$	(B-8)
	θ : 0	
Vortex	x : $2\pi \cos\alpha$	
	y : $2\pi \sin\alpha$	

In the formulas below the notation of the left sides is chosen to be consistent with [6], [7].

Axisymmetric Source

$$\left(\frac{\partial\phi}{\partial x}\right)_p = \sigma_j \left\{ 2 \sin\alpha \left(\cos\alpha - 2C\right) S' + \left(\frac{1}{12} \sin\alpha \cos\alpha \left[\sin^2\alpha + \frac{13}{6} + \ln\frac{S'}{8} \right] \right.\right.$$

$$\left.\left. + \frac{C}{16} \sin\alpha \left[\sin^2\alpha + \frac{3}{2} - 2\cos\alpha + 8 \ln S' - \ln 8 - 4C(1+\cos\alpha) \right] \right) S'^3 \right\}$$

$$+ \sigma_j^{(1)} \overline{y} \left\{ 4 \cos\alpha\, S' + \left(-\frac{\cos\alpha}{36} \left[6 \sin^2\alpha + 7 + 6 \ln\frac{S'}{8} \right] \right.\right.$$

$$\left.\left. + \frac{2C}{3} \left[\cos^2\alpha - 2 \sin^2\alpha - 2C \cos\alpha \right] \right) S'^3 \right\}$$

$$+ \sigma_j^{(2)} \overline{y}^2 \left\{ \frac{2}{3} \sin\alpha \left(\cos\alpha - 2C \right) S'^3 \right\} \qquad \text{(B-9)}$$

$$\left(\frac{\partial \phi}{\partial y}\right)_p = \sigma_j \left\{ \left(2 \sin^2\alpha + 2 \ln \frac{S'}{8} + 4C \cos \alpha\right) S' \right.$$

$$+ \left(\frac{1}{24} \left[2 \sin^4\alpha + 3 \sin^2\alpha - 3 - 3 \ln \frac{S'}{8} \right] \right.$$

$$\left. \left. + \frac{C}{12} \left[- \cos \alpha \, (6 \sin^2\alpha + \frac{11}{3} + 3 \ln 8) - 4 + 2 \ln S' + 8C(1 - 2C \cos \alpha) \right] \right) S'^3 \right\}$$

$$+ \sigma_j^{(1)} \bar{y} \left\{ 4 \sin \alpha S' + \left(\sin \alpha \left[-6 \sin^2\alpha - 11 + 6 \ln \frac{S'}{8} \right] + \frac{4}{3} C \sin\alpha \left[\cos\alpha - C \right] \right) S'^3 \right\}$$

$$+ \sigma_j^{(2)} \bar{y}^2 \left\{ \frac{2}{3} \left(\sin^2\alpha + \frac{2}{3} + \ln \frac{S'}{8} + 2C \cos \alpha \right) S'^3 \right\} \qquad \text{(B-10)}$$

Cross-Flow Source

$$\left(\frac{\partial \phi}{\partial x}\right)_p = \sigma_j \left\{ 2 \sin \alpha \left(\cos \alpha - 2C \right) S' \right.$$

$$+ \left(2 \sin\alpha \cos \alpha \left[2 \sin^2\alpha - 9 - 6 \ln \frac{S'}{8} \right] \right.$$

$$+ \frac{C}{12} \left[\sin\alpha \, (-6 \sin^2\alpha + 4 \sin \alpha - 5 + 6 \ln 8 - 4 \cos^2\alpha) \right.$$

$$\left. \left. + 2 - 6 \ln S' - 16C \sin \alpha \, (\cos \alpha - C) \right] \right) S'^3 \right\}$$

$$+ \sigma_j^{(1)} \bar{y} \left\{ 4 \cos\alpha \, S' + \left(\frac{1}{12} \cos \alpha \left[-2 \sin^2\alpha + 3 + 6 \ln \frac{S'}{8} \right] \right. \right.$$

$$\left. \left. + \frac{2C}{3} \left[\cos^2\alpha - \sin^2\alpha - 2C \sin \alpha \right] \right) S'^3 \right\}$$

$$+ \sigma_j^{(2)} \bar{y}^2 \left\{ \frac{2}{3} \sin\alpha \left(\cos \alpha - 2C \right) S'^3 \right\} \qquad \text{(B-11)}$$

$$\left(\frac{\partial\phi}{\partial y}\right)_p = \sigma_j\Bigg\{\left(2\sin^2\alpha + 4 + 2\ln\frac{S'}{8} + 4C\right)S'$$

$$+\left(\frac{1}{72}\left[\sin^2\alpha\,(6\sin^2\alpha - 43 - 24\ln\frac{S'}{8}) + 9 + 27\ln\frac{S'}{8}\right]\right.$$

$$\left.+\frac{C}{6}\left[\cos\alpha(-3\sin^2\alpha + 7 + 5\ln\frac{S'}{8}) - 1 + 4C\cos\alpha(\cos\alpha - 2C)\right]\right)S'^3\Bigg\}$$

$$+\sigma_j^{(1)}\overline{y}\Bigg\{4\sin\alpha S' + \left(\frac{\sin\alpha}{36}\left[-6\sin^2\alpha + 29 + 30\ln\frac{S'}{8}\right]\right.$$

$$\left.+\frac{4}{3}C\sin\alpha\left[\cos\alpha - C\right]\right)S'^3\Bigg\}$$

$$+\sigma_j^{(2)}\overline{y}^2\left\{\frac{2}{3}\left(\sin^2\alpha + \frac{8}{3} + \ln\frac{S'}{8} + 2C\cos\alpha\right)S'^3\right\} \qquad \text{(B-12)}$$

$$\left(\frac{1}{y}\frac{\partial\phi}{\partial\theta}\right)_p = \sigma_j\left\{-4\left(1 + \ln\frac{S'}{8}\right)S' + \left(\frac{1}{36}\left[10\sin^2\alpha + (6\sin^2\alpha - 9)\ln\frac{S'}{8}\right]\right.\right.$$

$$\left.\left.+\frac{C}{9}\left[-4\cos\alpha + 6 - 6\cos\alpha\ln\frac{S'}{8}\right]\right)S'^3\right\}$$

$$+\sigma_j^{(1)}\overline{y}\left\{-\frac{2}{3}\sin\alpha\left(\frac{4}{3} + \ln\frac{S'}{8}\right)S'^3\right\} + \sigma_j^{(2)}\overline{y}^2\left\{-\frac{4}{3}\left(\frac{5}{3} + \ln\frac{S'}{8}\right)S'^3\right\} \qquad \text{(B-13)}$$

Axisymmetric Vorticity

$$V_x'\,(\text{vortex}) = \left(-2\sin^2\alpha + 2\ln\frac{S'}{8} - 4C\cos\alpha\right)S'$$

$$+\left(\left[\frac{1}{72}\sin^2\alpha\,(-6\sin^2\alpha - 72\cos\alpha + 23 + 12\ln\frac{S'}{8}) - \frac{1}{8}(1 + \ln\frac{S'}{8})\right]\right.$$

$$+\frac{C}{36}\left[\cos\alpha(54\sin^2\alpha - 11 + 6\ln 8 + 30\ln S') - 12\right.$$

$$\left.\left.+24C\,(3\sin^2\alpha - \cos^2\alpha - C\cos\alpha)\right]\right)S'^3 \qquad \text{(B-14)}$$

$$V'_y \text{ (vortex)} = \left(2 \sin \alpha \left[\cos \alpha - 2C \right] \right) S'$$

$$- \left(\frac{1}{24} \sin \alpha \cos \alpha \left[-2 \sin^2 \alpha + 9 + 6 \ln \frac{S'}{8} \right] \right.$$

$$+ \frac{C}{12} \sin \alpha \left[66 \sin^2 \alpha + 31 - 12 \cos^2 \alpha + \frac{32}{3} \ln S' \right.$$

$$\left. \left. - 18 \ln 8 + 48C \cos \alpha \right] \right) S'^3 \qquad \text{(B-15)}$$

APPENDIX C
NUMERICAL DIFFERENTIATION FORMULAS

First the options must be applied as follows:

Constant Source Option — set $\vec{V}_{ij}^{(1)} = \vec{V}_{ij}^{(2)} = 0$

Linear Source Option — set $\vec{V}_{ij}^{(2)} = 0$

Now for any element that is not the first or last of a body, compute the quantities

$$D_j = \frac{-1}{2[s'_j + 1/2(s'_{j-1} + s'_{j+1})]} \cdot \frac{s'_j + s'_{j+1}}{s'_j + s'_{j-1}}$$

$$E_j = \frac{1}{2[s'_j + 1/2(s'_{j-1} + s'_{j+1})]} \cdot \left[\frac{s'_j + s'_{j+1}}{s'_j + s'_{j-1}} - \frac{s'_j + s'_{j-1}}{s'_j + s'_{j+1}}\right]$$

$$F_j = \frac{1}{2[s'_j + 1/2(s'_{j-1} + s'_{j+1})]} \cdot \frac{s'_j + s'_{j-1}}{s'_j + s'_{j+1}} \qquad \text{(C-1)}$$

$$G_j = \frac{1}{2[s'_j + 1/2(s'_{j-1} + s'_{j+1})](s'_j + s'_{j-1})}$$

$$H_j = \frac{-1}{(s'_j + s'_{j-1})(s'_j + s'_{j+1})}$$

$$I_j = \frac{1}{2[s'_j + 1/2(s'_{j-1} + s'_{j+1})](s'_j + s'_{j+1})}$$

where the "half arc length" s' of an element is defined in Appendix A. These are used in (11).

When computing the effect of the first (j=1) element of each body, (11) is replaced by

$$\sigma_1^{(1)} = A\sigma_1 + B\sigma_2 + C\sigma_3$$

$$\sigma_1^{(2)} = G_2\sigma_1 + H_2\sigma_2 + I_2\sigma_3 \qquad \text{(C-2)}$$

Here the quantities G_2, H_2, I_2 are given by (C-1) with j=2, i.e., they are the same as the second element's (but they multiply different quantities). The new quantities are

$$A = -\frac{s_2' + s_1' + 1/2(s_2' + s_3')}{(s_2' + s_1')[s_2' + 1/2(s_1' + s_3')]}$$

$$B = 2\frac{s_2' + 1/2(s_1' + s_3')}{(s_1' + s_2')(s_2' + s_3')} \qquad \text{(C-3)}$$

$$C = -\frac{1}{2}\frac{s_1' + s_2'}{(s_2' + s_3')[s_2' + 1/2(s_1' + s_3')]}$$

When computing the effect of the last element on a body, say j=L, (11) is replaced by

$$\sigma_L^{(1)} = X\sigma_{L-2} + Y\sigma_{L-1} + Z\sigma_L$$

$$\sigma_L^{(2)} = G_{L-1}\sigma_{L-2} + H_{L-1}\sigma_{L-1} + I_{L-1}\sigma_L \qquad \text{(C-4)}$$

where the quantities G_{L-1}, H_{L-1}, I_{L-1} are given by (C-1) with j=L-1, i.e., the same as the preceding element (but used differently). The new quantities are

$$X = \frac{1}{2}\frac{s_{L-1}' + s_L'}{(s_{L-2}' + s_{L-1}')[s_{L-1}' + 1/2(s_{L-2}' + s_L')]}$$

$$Y = -2\frac{s_{L-1}' + 1/2(s_{L-2}' + s_L')}{(s_{L-2}' + s_{L-1}')(s_{L-1}' + s_L')} \qquad \text{(C-5)}$$

$$Z = \frac{s_{L-1}' + s_L' + 1/2(s_{L-1}' + s_{L-2}')}{(s_{L-1}' + s_L')[s_{L-1}' + 1/2(s_{L-2}' + s_L')]}$$

APPENDIX D

BASIC SOLUTIONS FOR INLETS AND SHROUDED PROPELLERS

A common application of the present method is the calculation of flow over the forward portions of inlets or propeller shrouds. In such cases a complication arises from the necessity of obtaining the desired total flow through the inlet — the so-called mass flow ratio. (The effect of all the interior machinery is lumped into this quantity.) The straightforward way to handle this problem is to simply define by input points a surface across the interior coinciding with the actual propeller plane or compressor face and to specify the desired mass flow as a nonzero normal velocity on this surface. This procedure fails for reasons related to the inability of the present method to handle internal corners. The calculated flow in the neighborhood of the simulated compressor face is erratic and not physically meaningful. Thus resort must be made to an artifice.

The forward portion of the inlet is artificially extended by means of long afterbodies with constant inner and outer diameters as shown in figure 9. A forward location is selected in the region where the flow is of interest, and it is designated the control station for mass flow ratio. Often the choice is the propeller plane or compressor face. Three fundamental flows are calculated. The first two are illustrated in figure 9. The long afterbody is left open at the rear and flows calculated for uniform onset flows at 0° and 90° angle of attack. The 0° flow gives a certain value of mass flow at the control station. This value cannot be predicted a priori, but it is usually near unity. The 90° flow is a cross flow and gives zero net flow through the control station. These two solutions can be combined to give an onset flow at any angle of attack, but the mass flow ratio is always that obtained from the 0° onset flow. To obtain other mass flow ratios a third basic flow is required.

The third basic flow is that for the inlet in static operation. That is, the flow is zero at infinity but has a finite mass flow at the control station. This flow can be linearly combined with the first two to give the flow about the inlet at any angle of attack and any mass flow ratio at the control station. Thus all solutions are obtained from the basic three.

It is the third solution for static operation that leads to numerical difficulty. Two methods of obtaining it are illustrated in figure 10. The most straightforward procedure is that illustrated in figure 10a. A surface is placed across the interior of the inlet far back in the constant diameter region, and a nonzero normal velocity is prescribed on this "suction" surface. The flow in the neighborhood of the surface is meaningless as described above, but it smooths out upstream and is well-behaved at the control station. The mass flow obtained at the control station may be different than that specified on the suction surface, due to "leakage" caused by numerical errors. However, since this solution is to be linearly combined with other solutions, the exact value of mass flow is unimportant. This value is essentially absorbed in the combination constant.

The solution of figure 10a gives good results inside the inlet and around the lip, but inaccuracies enter in the exterior region. Because a finite number of surface elements are used, the exterior flow "sees through" the inlet surface directly to the suction surface and is pulled towards that surface. Thus as shown in figure 10a there is a stagnation point on the exterior surface. Fluid to the left enters the inlet mouth, while fluid on the right flows aft along the inlet. For the exact solution, which could be approached by using a very large number of elements, the inlet surfaces "screen out" the suction element from the exterior flow, and the suction effect is felt solely through the inlet mouth. Thus the actual flow is to the left over the entire exterior surface with the velocity falling rapidly to zero with increasing distance from the inlet mouth. The calculated velocity is not large, but it is in the wrong direction in this region.

For the exterior region, the scheme shown in figure 10b gives a more accurate solution for static operation. A constant unit strength vorticity distribution is taken to lie on the surface. Of course, the normal velocity on the body due to the vorticity distribution is not zero, and a surface source distribution is also required. The flow field of the constant vorticity distribution provides another onset flow to the body, and the values of source density on the elements are determined in the usual way to give zero normal velocity at all control points in the presence of the vorticity distribution. The only difference between this flow solution and the solution for a uniform onset flow is the right side of the linear equations. (This device also provides lift for airfoils [4], although for axisymmetric inlets the vorticity is ring vorticity.) It can be shown that if the afterbodies are infinitely long, even with finite-element lengths, the solution obtained in this manner is the correct static solution. Specifically, there is constant flow far back inside and outside a leftward flow that falls to zero with increasing distance from the inlet lip (figure 10b). The error in this case arises from the fact that long finite afterbodies lead to small nonzero velocities on the exterior surface, but this velocity is in the right direction.

REFERENCES

1. Hess, J. L.: Review of Integral-Equation Techniques for Solving Potential-Flow Problems with Emphasis on the Surface-Source Method. Douglas Aircraft Co. Engineering Paper No. 6287, May 1974.

2. Hess, J. L. and Smith, A. M. O.: Calculation of Potential Flow About Arbitrary Bodies. Prog. in Aero. Sci., Vol. 8, Pergamon Press, New York, 1966.

3. Hess, J. L.: Higher-Order Numerical Solution of the Integral Equation for the Two-Dimensional Neumann Problem. Computer Methods in Applied Mech. and Engg., Vol. 2, No. 1, Feb. 1973, pp. 1-15.

4. Hess, J. L.: The Use of Higher-Order Surface Singularity Distributions to Obtain Improved Potential Flow Solutions for Two-Dimensional Lifting Airfoils. Douglas Aircraft Co. Engineering Paper No. 6268, June 1974.

5. Argyris, J. H.: The Impact of the Digital Computer on Engineering Sciences. Twelfth Lanchester Memorial Lecture. The Aero. Journal of the Royal Aero. Society, Vol. 74, Nos. 709, 710, Jan., Feb. 1970.

6. Smith, A. M. O. and Pierce, J.: Exact Solution of the Neumann Problem. Calculation of Plane and Axially Symmetric Flows about or within Arbitrary Boundaries. Douglas Aircraft Co. Report No. 26988, Apr. 1958. (A brief summary is contained in the Proceedings of the Third U. S. National Congress of Applied Mechanics, Brown University, 1958.)

7. Hess, J. L.: Calculation of Potential Flow about Bodies of Revolution Having Axes Perpendicular to the Free-Stream Direction. J. of the Aero-space Sciences, Vol. 29, No. 6, 1962, p. 726.

8. Hess, J. L.: Extension of the Douglas Axisymmetric Potential Flow Program to Include the Effects of Ring Vorticity with Application to the Problem of Specified Tangential Velocity. Douglas Aircraft Co. Report No. DAC 33195, June 1966.

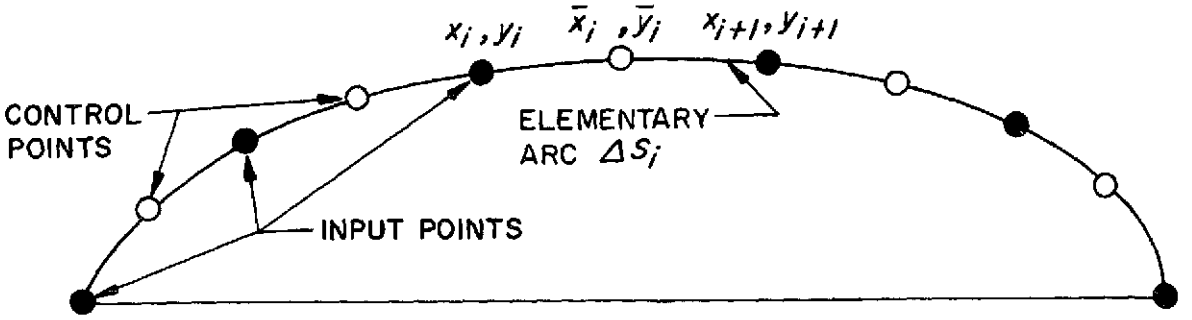

Figure 1. Division of a body contour into elementary arcs.

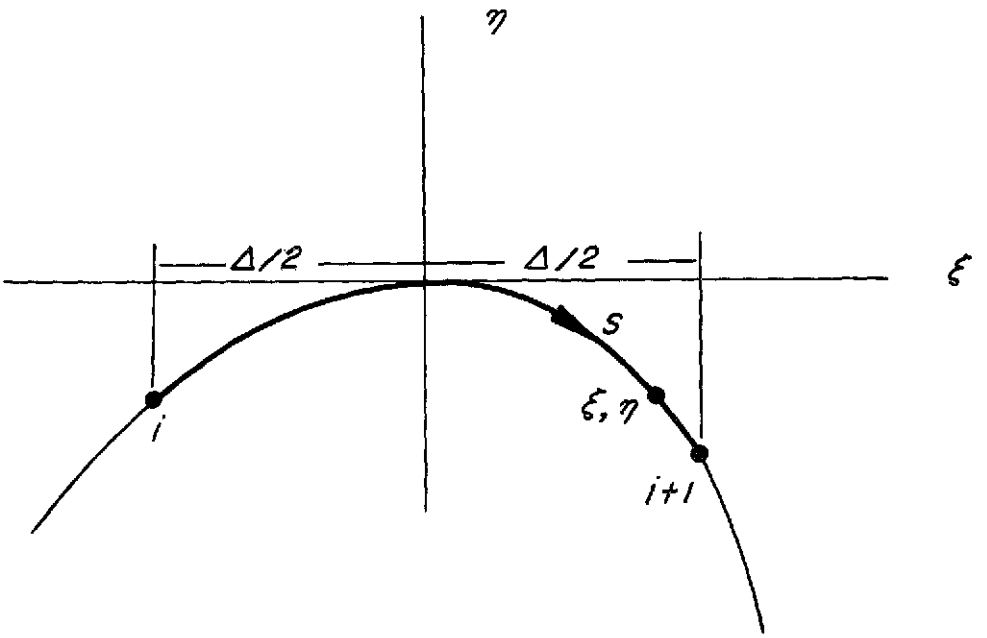

Figure 2. An elementary arc.

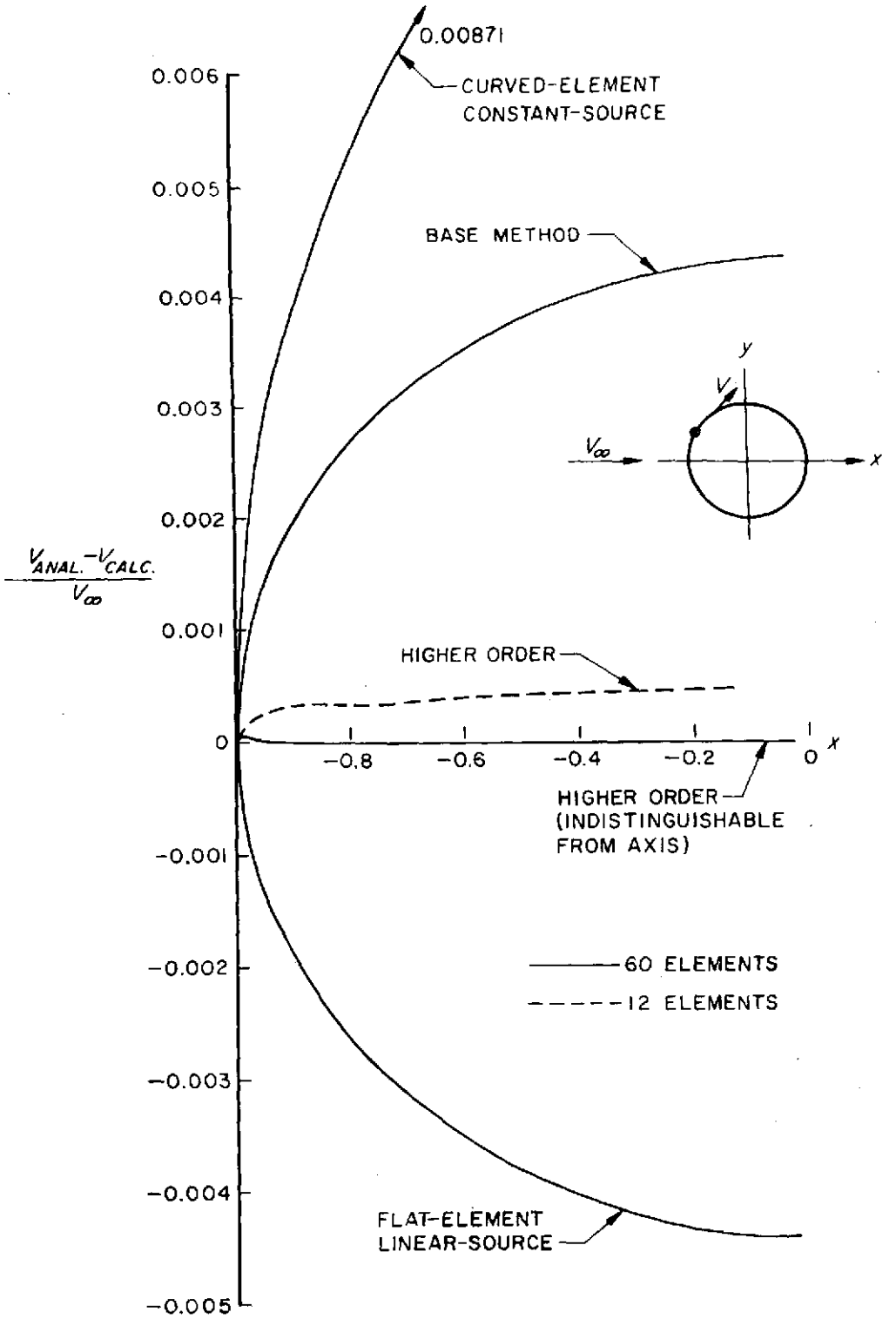

Figure 3. Errors in surface velocity calculated by various methods for a sphere in a uniform onset flow parallel to the x-axis.

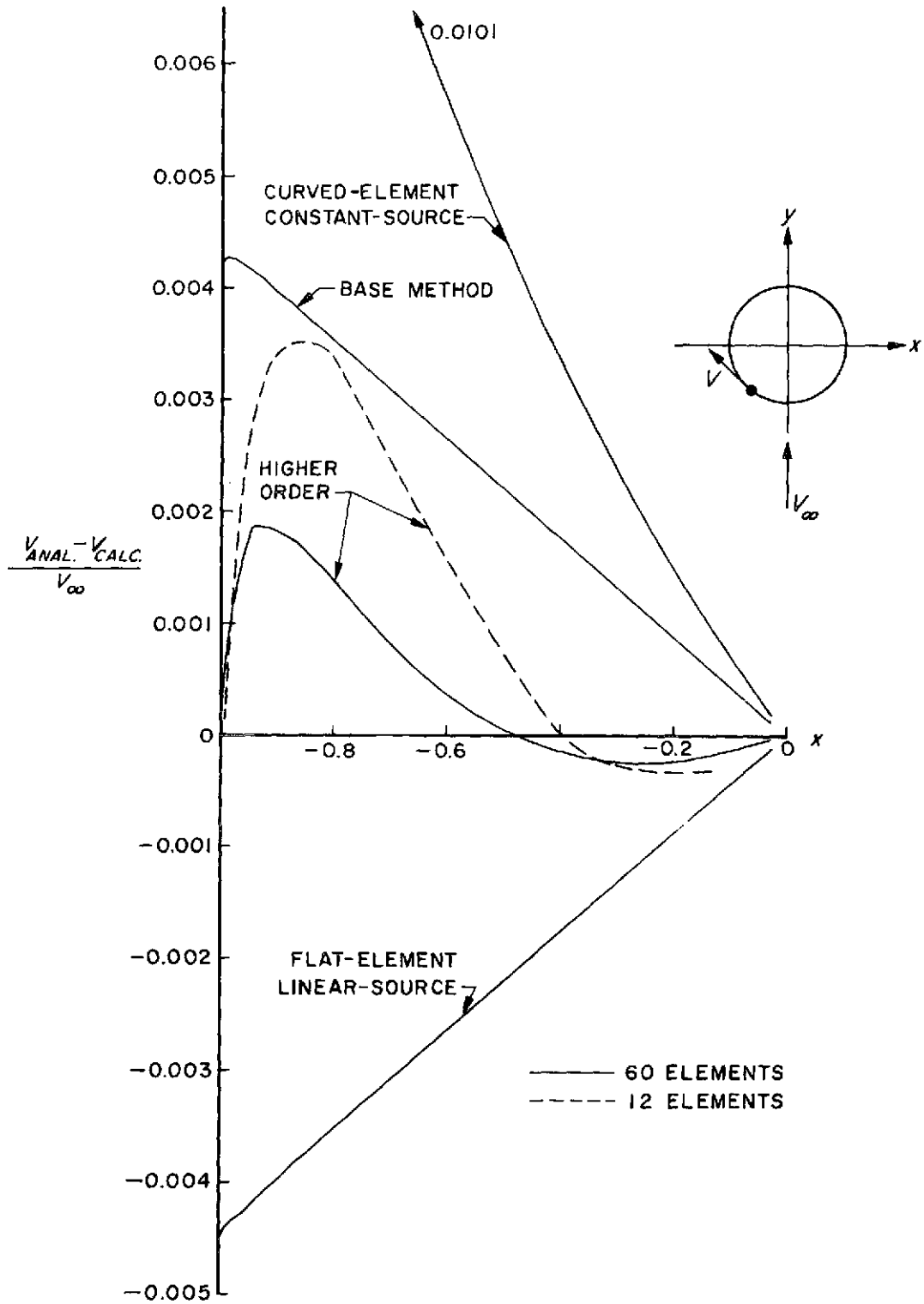

Figure 4. Errors in surface velocity calculated by various methods for a sphere in a uniform onset flow parallel to the y-axis. (a) Velocity in the xy-plane.

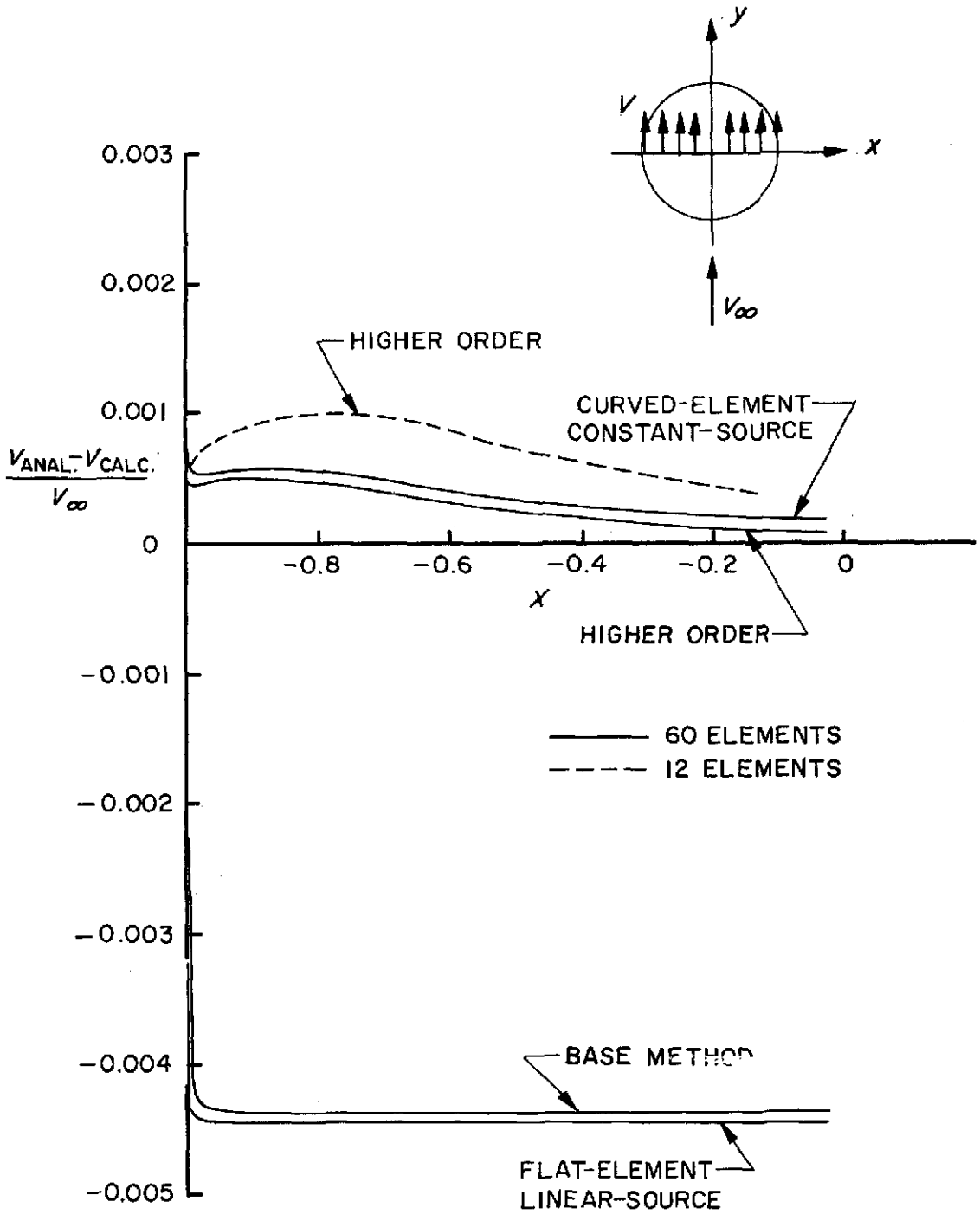

Figure 4. (b) Velocity in the xz-plane.

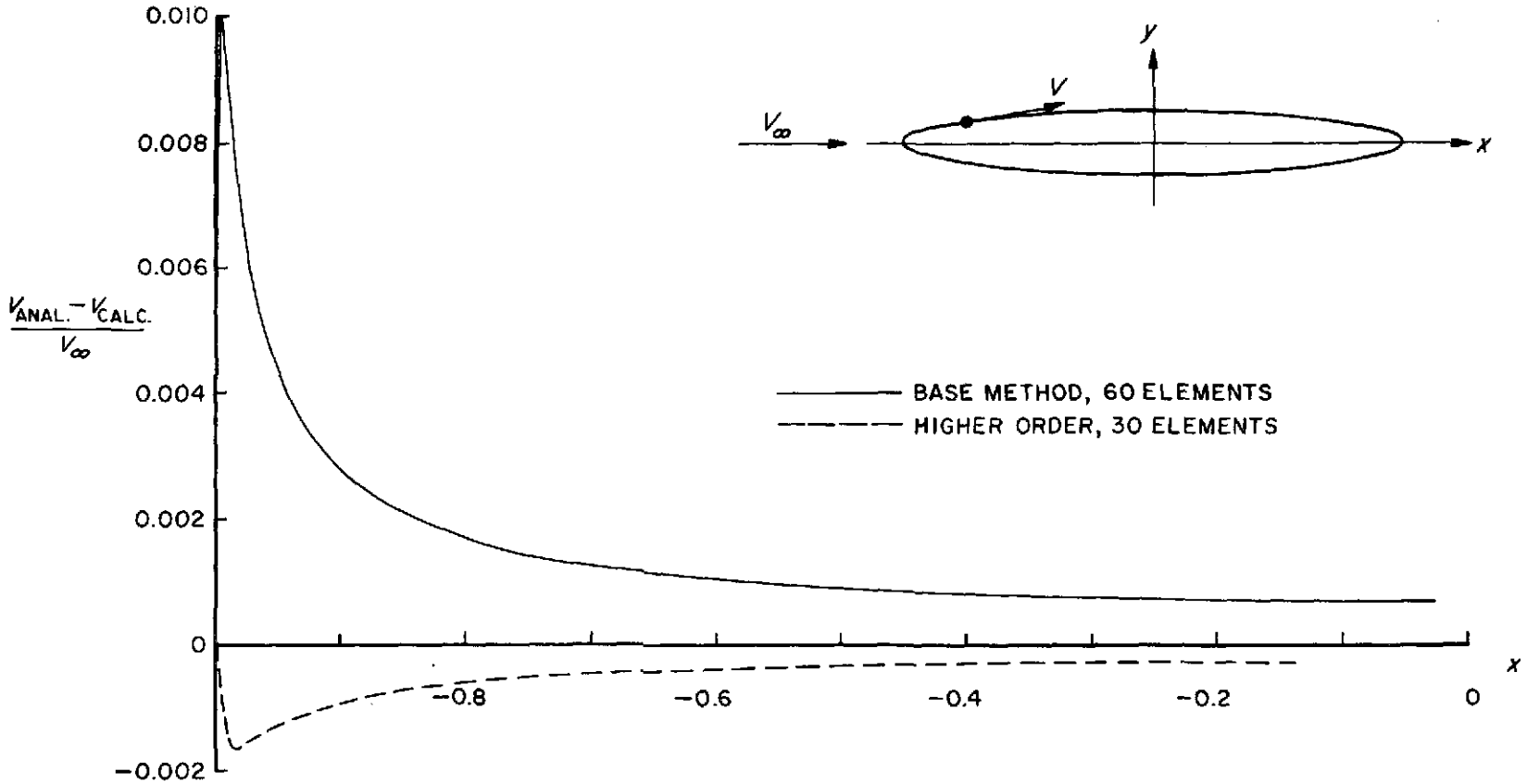

Figure 5. Errors in calculated surface velocity on an 8-to-1 prolate spheroid in a uniform onset flow parallel to the x-axis.

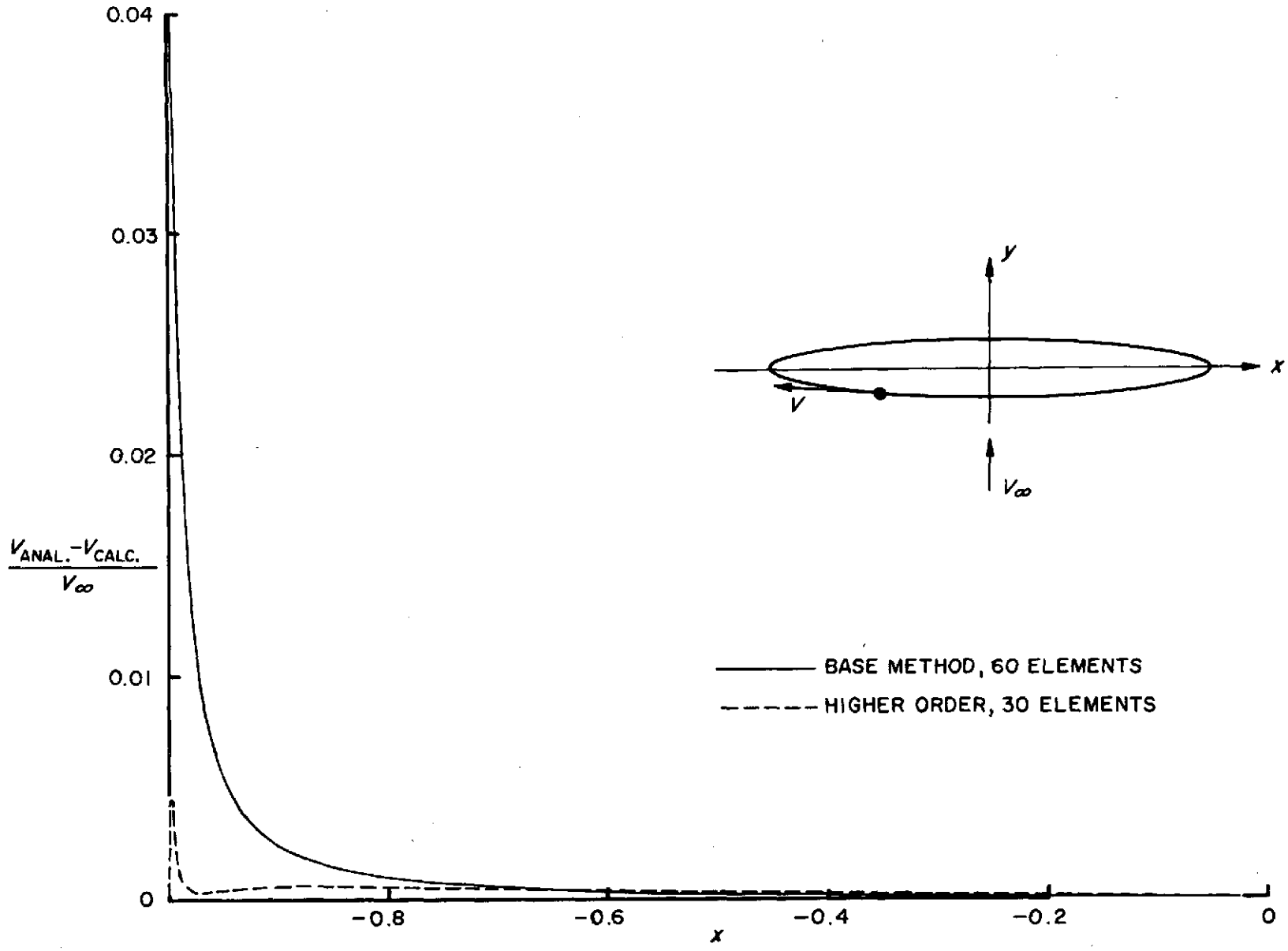

Figure 6. Errors in calculated surface velocity on an 8-to-1 prolate spheroid in a uniform onset flow parallel to the y-axis. (a) Velocity in the xy-plane.

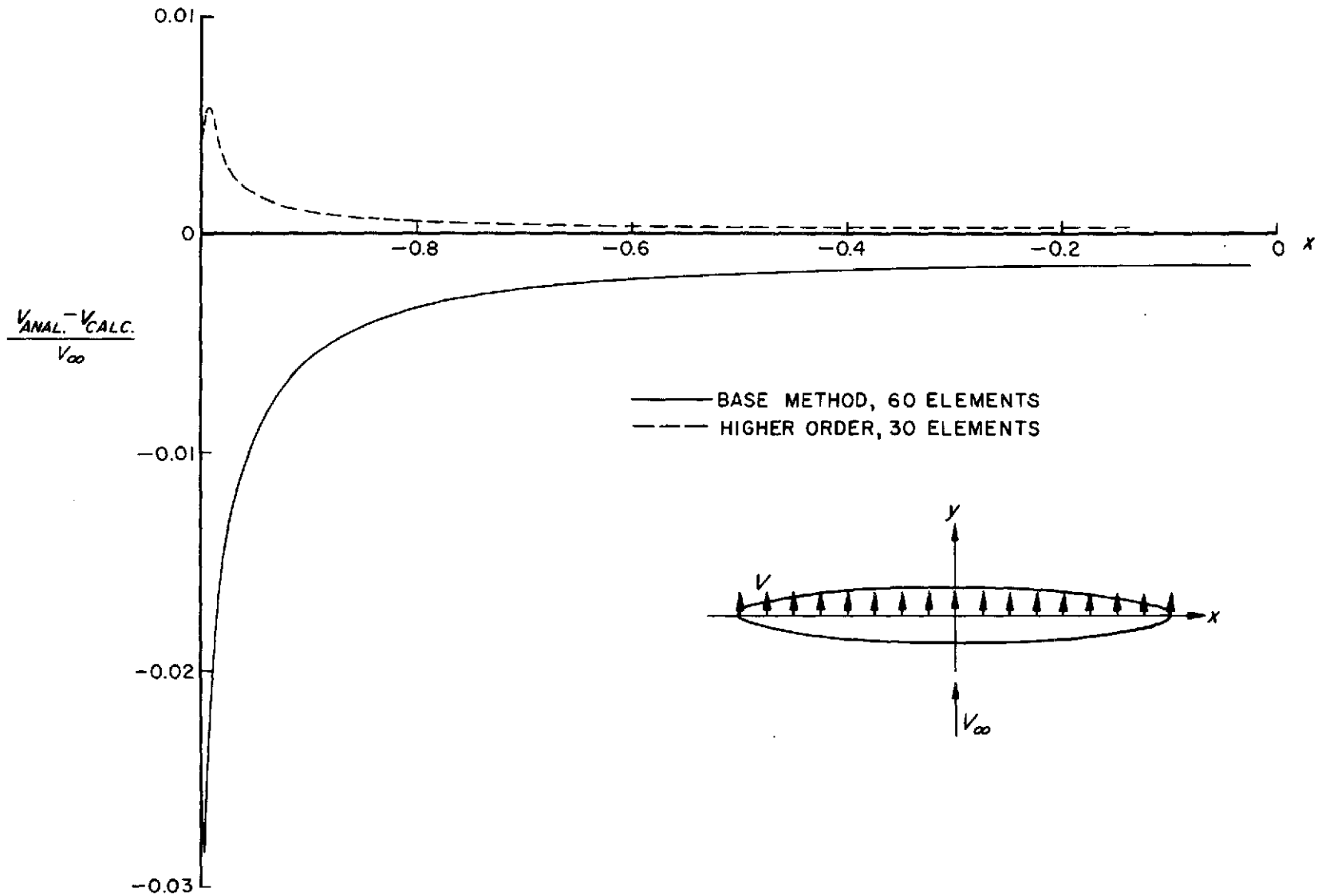

Figure 6. (b) Velocity in the xz-plane.

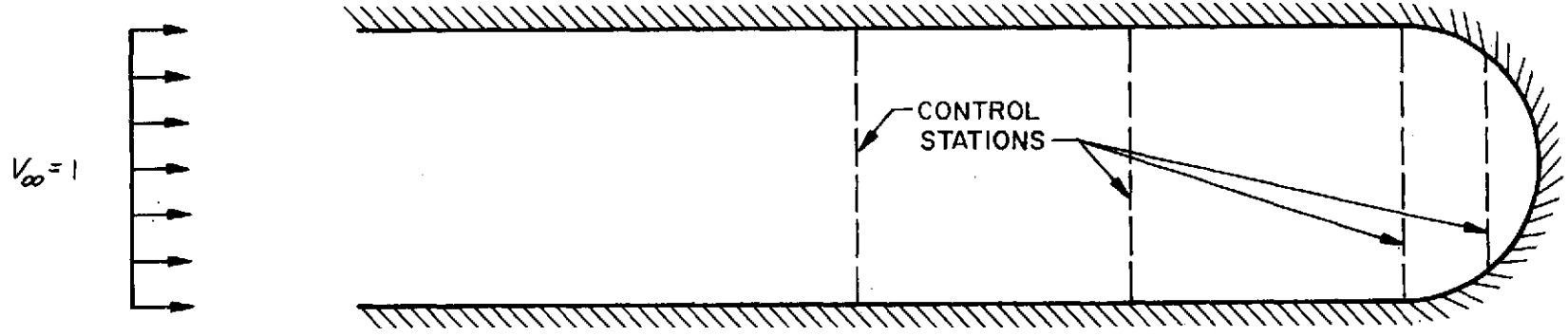

Figure 7. A closed duct showing control stations where average velocities are computed.

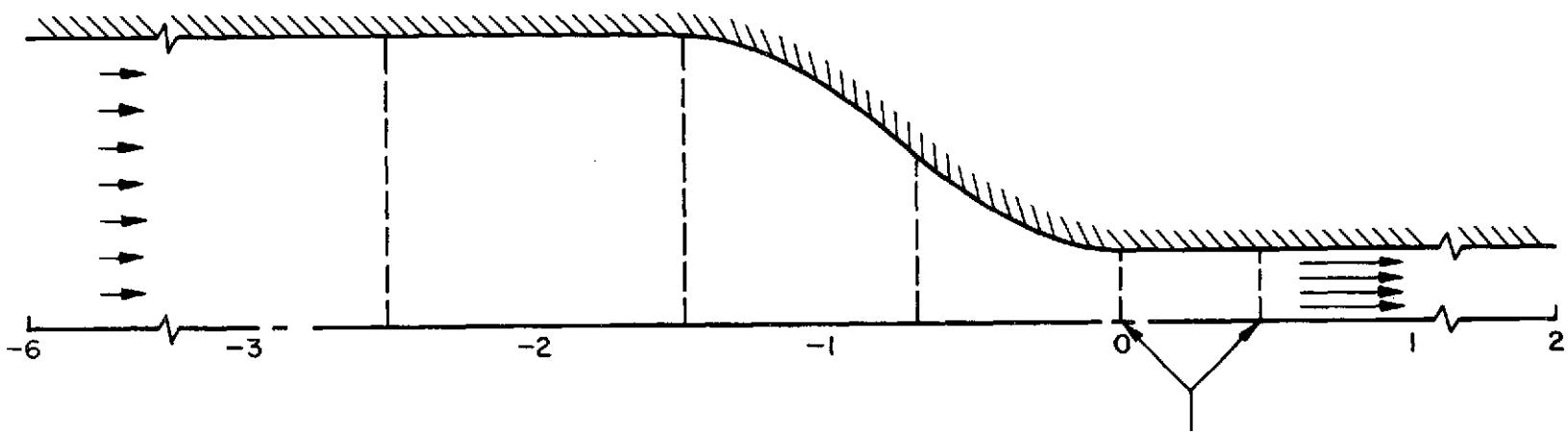

Figure 8. Flow in a contracting duct of area ratio 16 with total velocity fluxes calculated at various locations by the higher-order and base method.

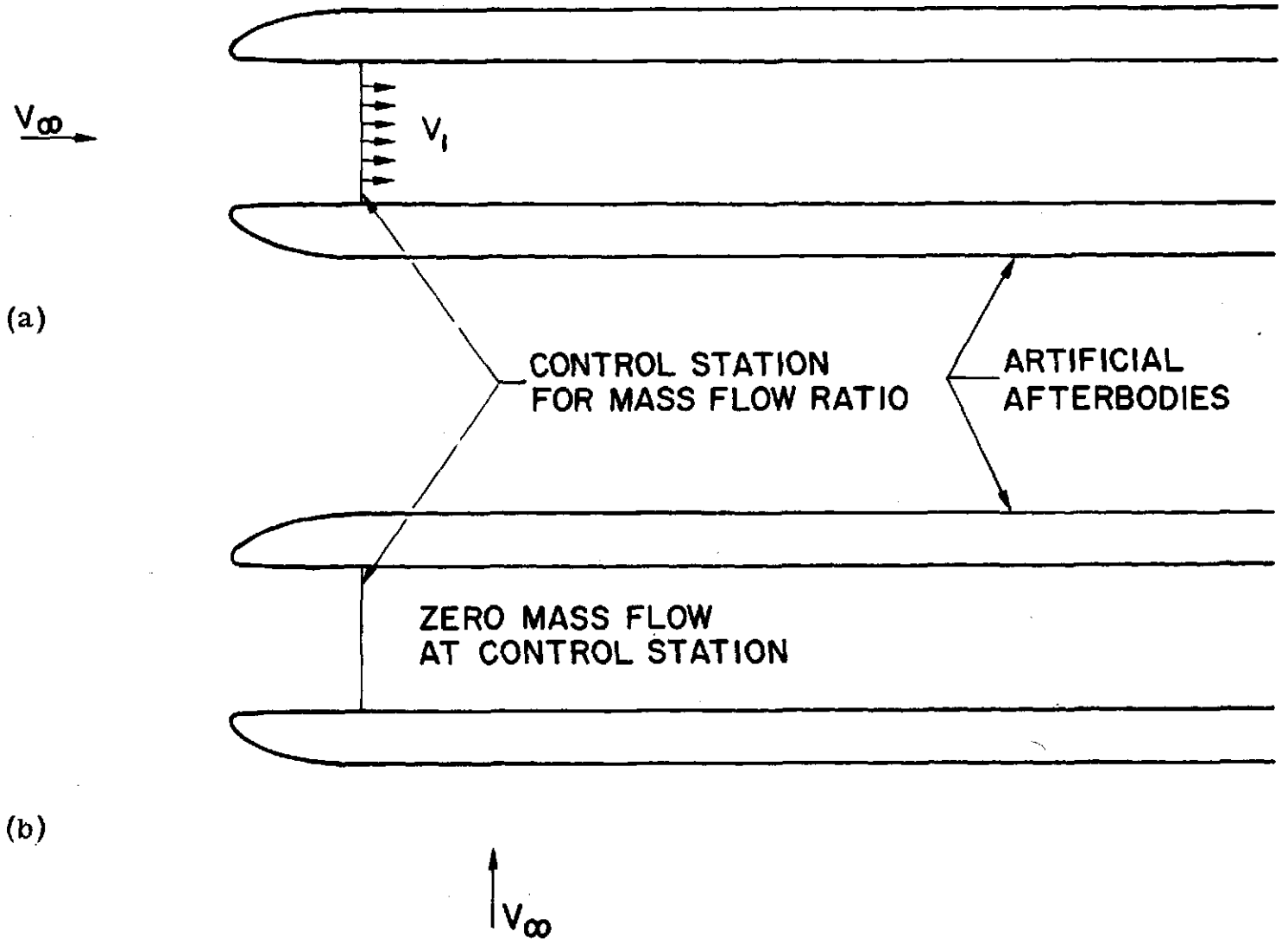

Figure 9 . Angle of attack solutions for inlets. (a) 0° angle of attack.
(b) 90° angle of attack.

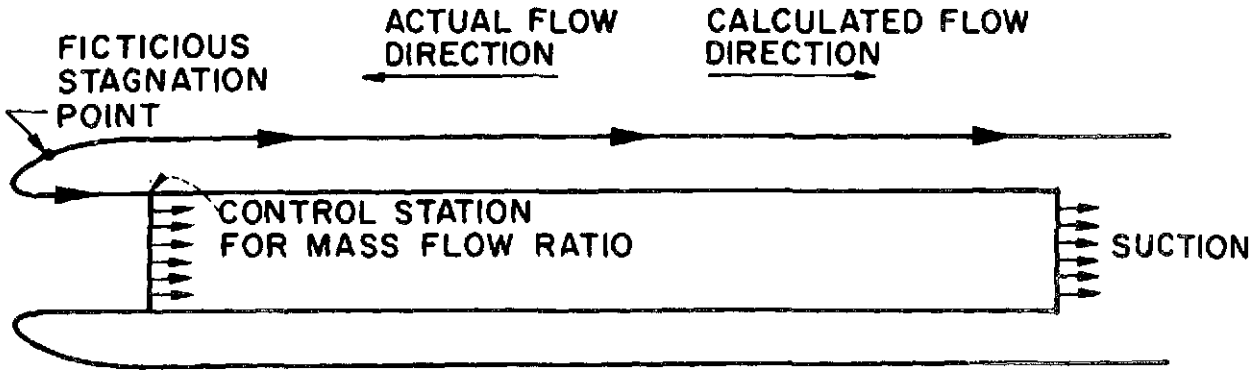

(a)

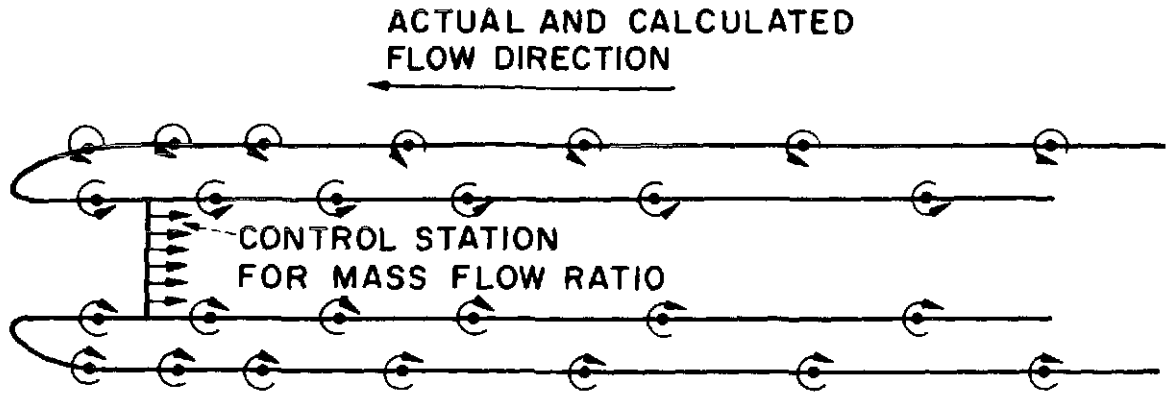

(b)

Figure 10. Two methods for simulating flow about an inlet in static operation. (a) Interior suction. (b) Surface vorticity.

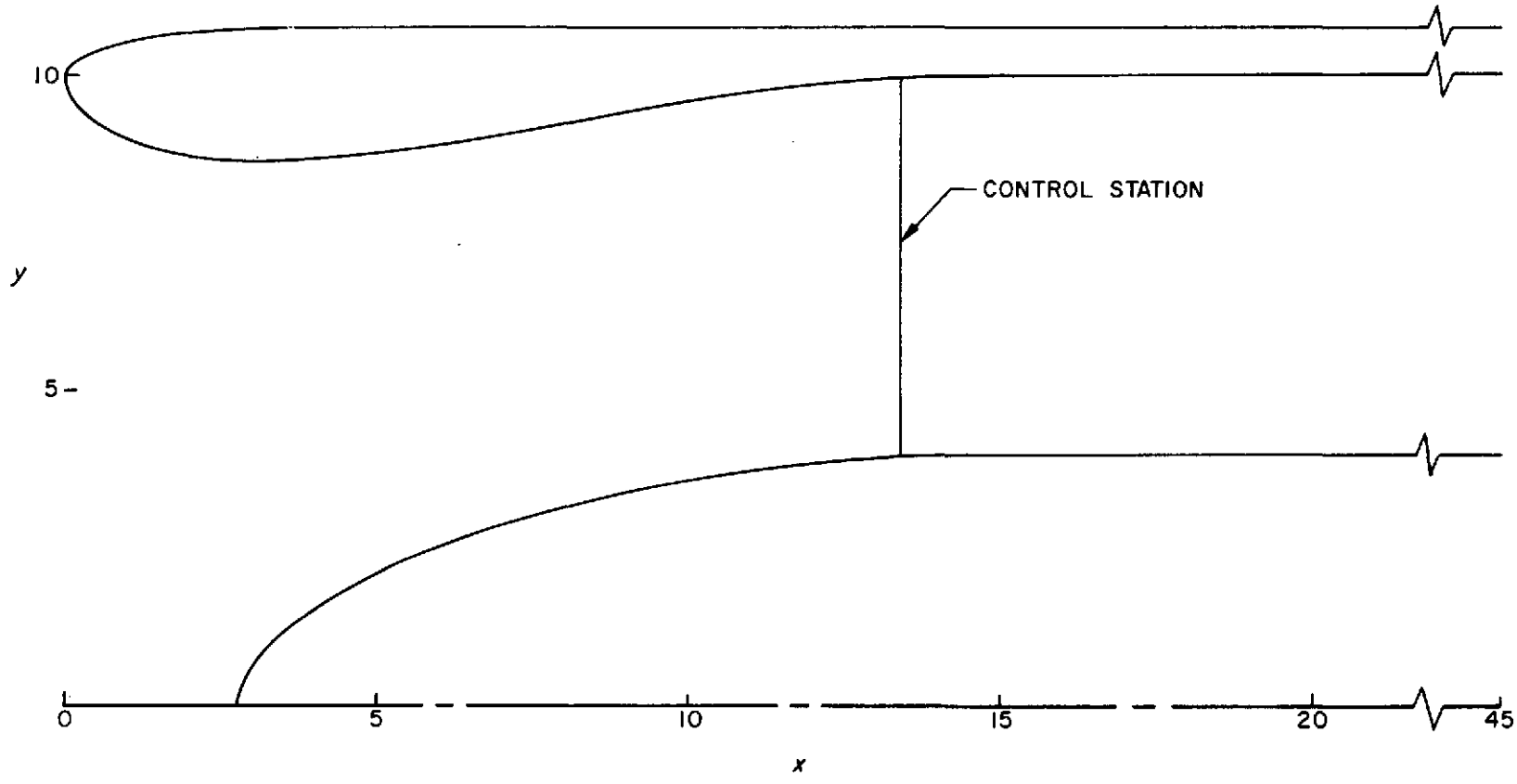

Figure 11. The inlet with centerbody for which calculated results are presented.

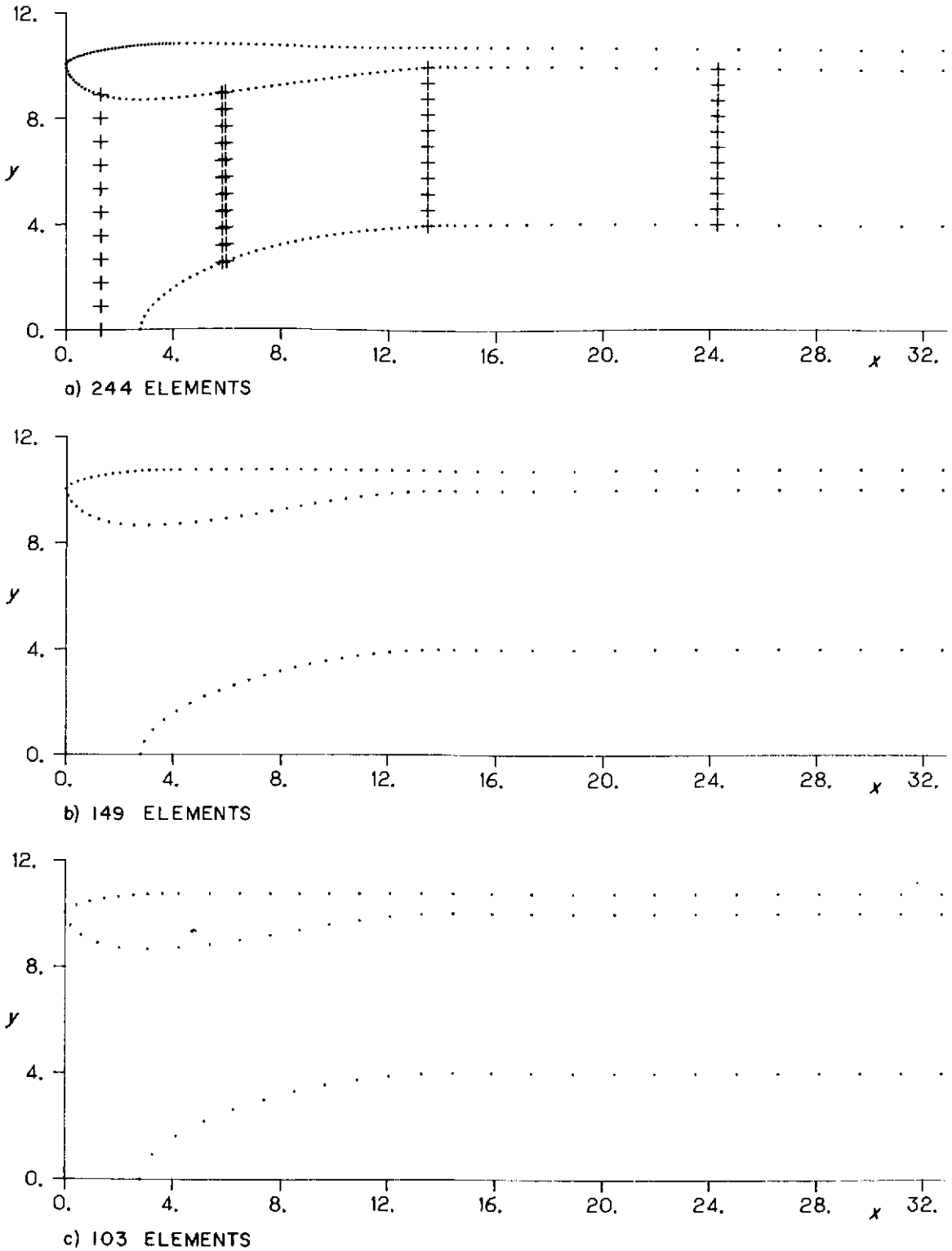

Figure 12. Three input point distributions on an inlet.

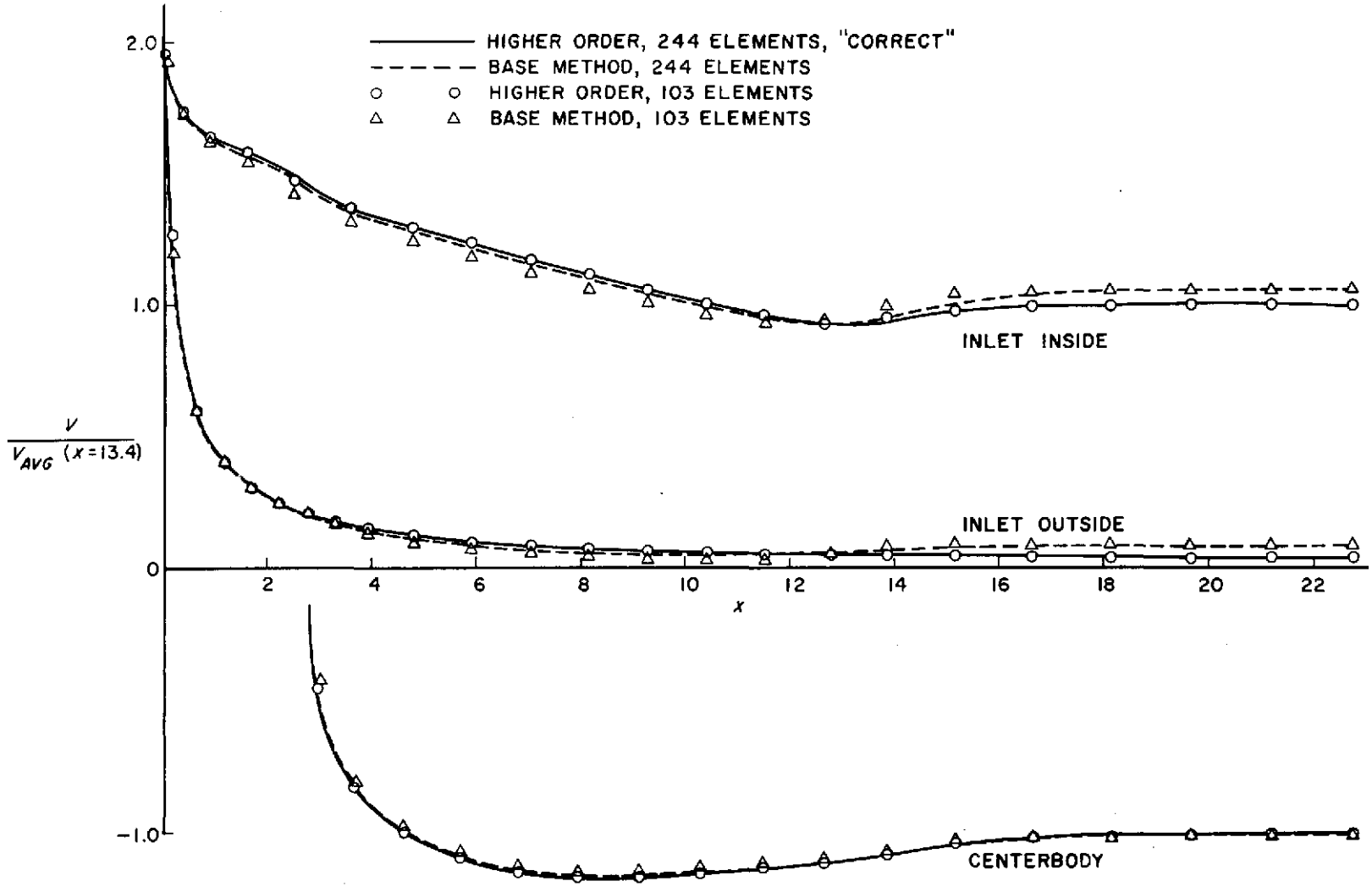

Figure 13. Calculated surface velocity distributions on an inlet in static operation simulated by a surface vorticity solution.

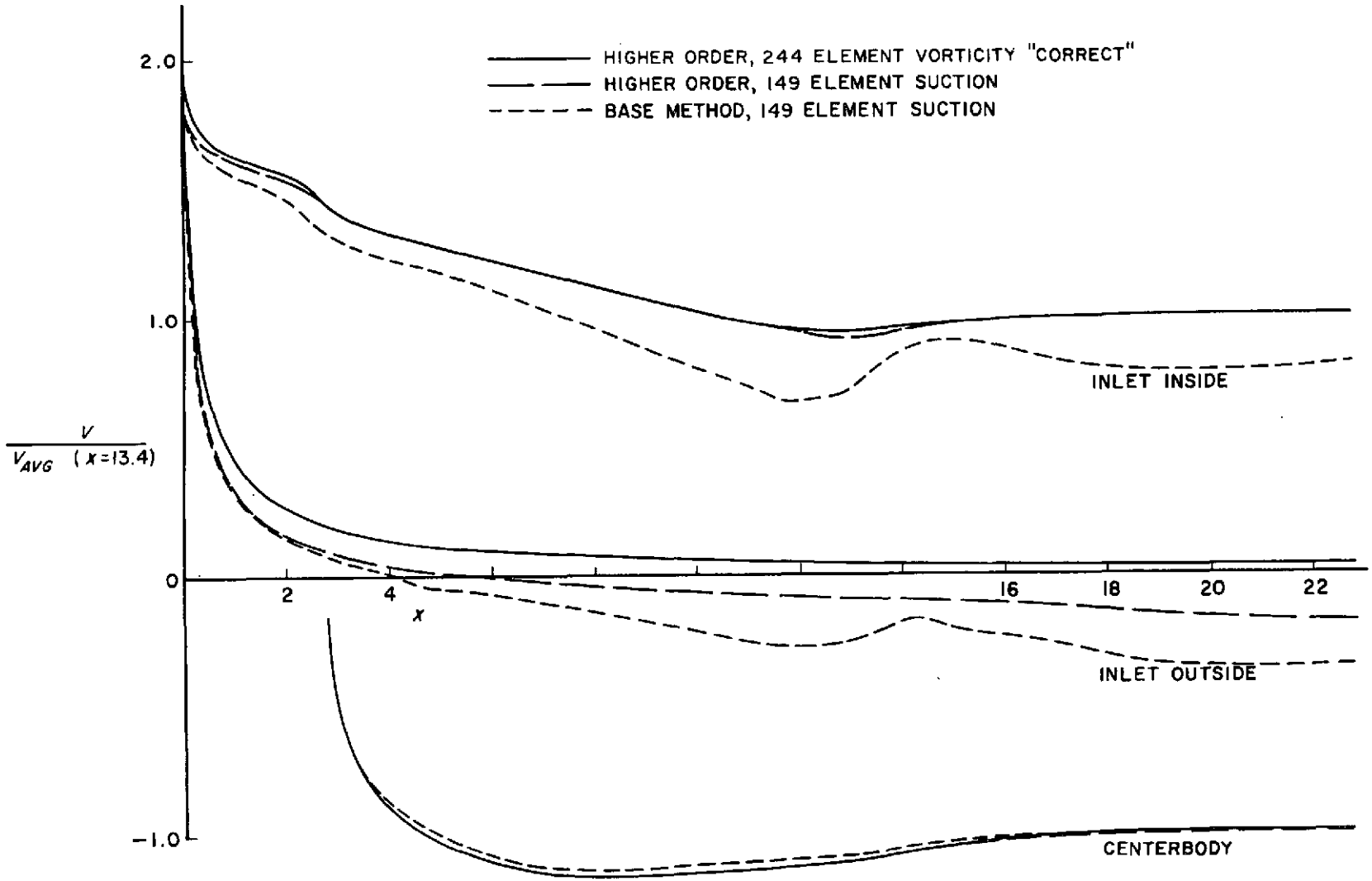

Figure 14. Comparison of calculated surface velocity distributions on an inlet in static operation simulated by the two methods.